



chem 5390

Advanced X-ray Analysis

LECTURE 15

**Dr. Teresa D. Golden
University of North Texas
Department of Chemistry**

Application of Diffraction Data

XRD can be used for:

- Bravais lattice determination – phase determination (crystalline phases and orientation)
- Lattice parameter determination
- Determination of solvus line in phase diagrams (order-disorder transformation)
- Long range order
- Crystallite size and Strain
- Temperature factor – thermal diffuse scattering (thermal expansion)
- Thickness measurements of thin films and multilayers

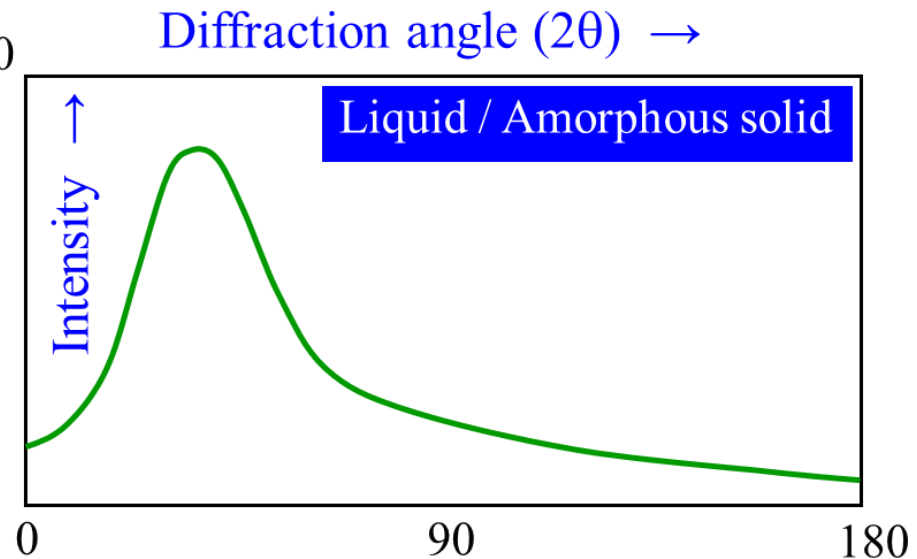
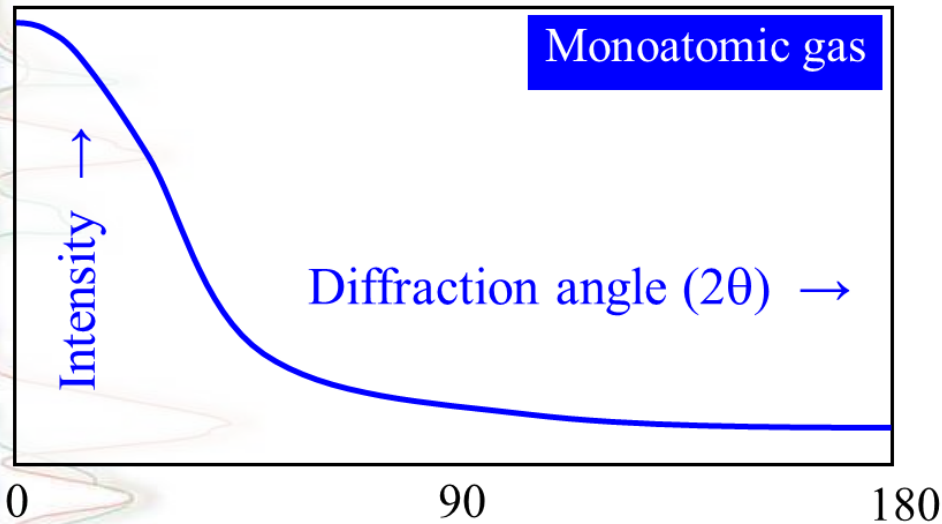
Application of Diffraction Data

XRD can be used for:

- Bravais lattice determination – phase determination (crystalline phases and orientation)**
- Lattice parameter determination**
- Determination of solvus line in phase diagrams (order-disorder transformation)**
- Long range order**
- Crystallite size and Strain**
- Temperature factor – thermal diffuse scattering (thermal expansion)**
- Thickness measurements of thin films and multilayers**

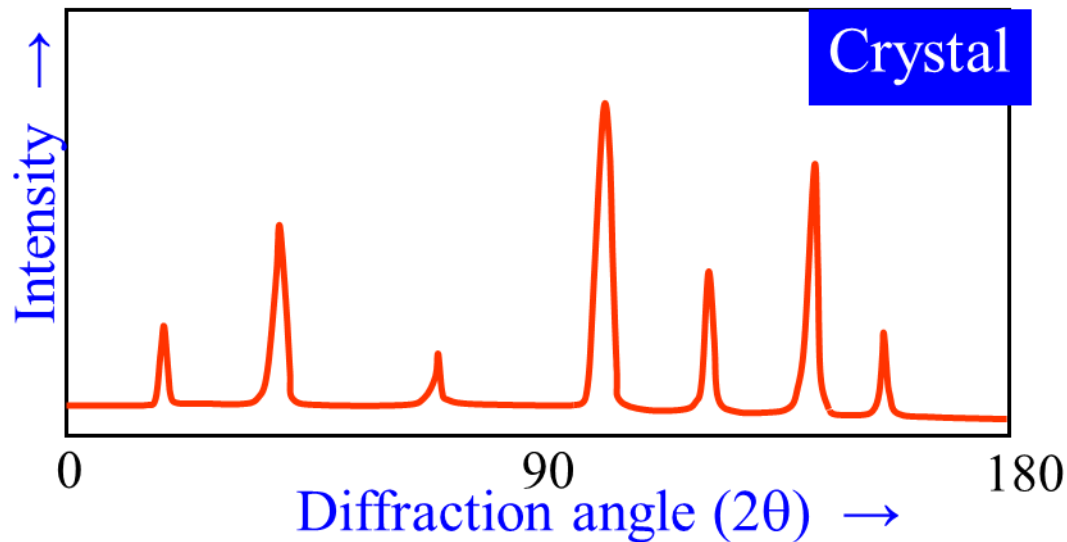
Application of Diffraction Data

Schematic of difference between the diffraction patterns of various phases



Application of Diffraction Data

Schematic of difference between the diffraction patterns of various phases – we are mostly interested in crystalline phases.



Bravais lattice determination – phase determination
(crystalline phases and orientation)

Application of Diffraction Data

Diffractometer (Powder) Method

Phase Analysis

When X-rays interact with a crystalline substance, the x-ray diffraction pattern of a substance is like a fingerprint of the substance.

It can be used for identification of the various crystalline compounds, known as 'phases', present in solid materials and powders.

The powder diffraction method is thus ideally suited for characterization and identification of polycrystalline phases.

The main use of powder diffraction is to identify components in a sample by a search/match procedure.

Application of Diffraction Data

Phase Analysis

When thousands of crystallites are sampled, for every set of planes, there will be a small percentage of crystallites that are properly oriented to diffract

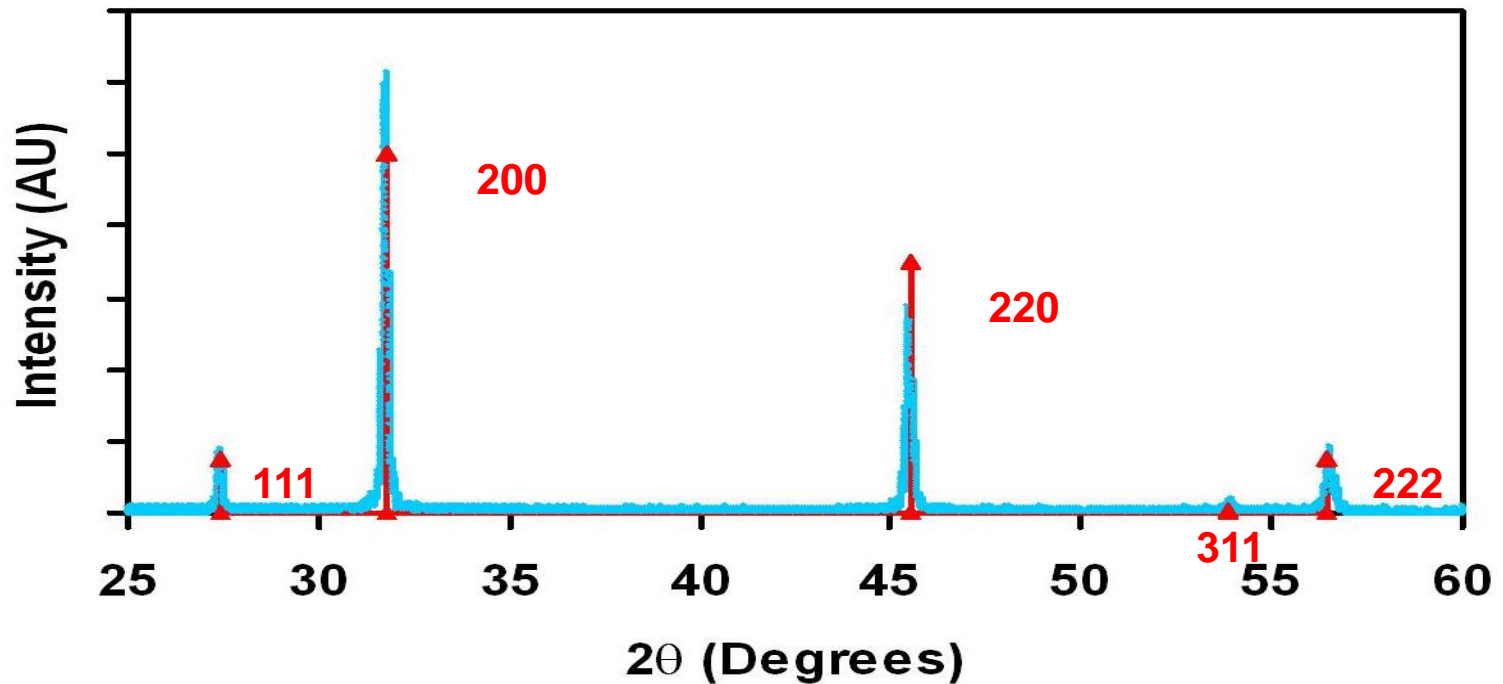
All possible diffraction peaks should be exhibited

Their intensities should match the powder diffraction file.

Application of Diffraction Data

Phase Analysis

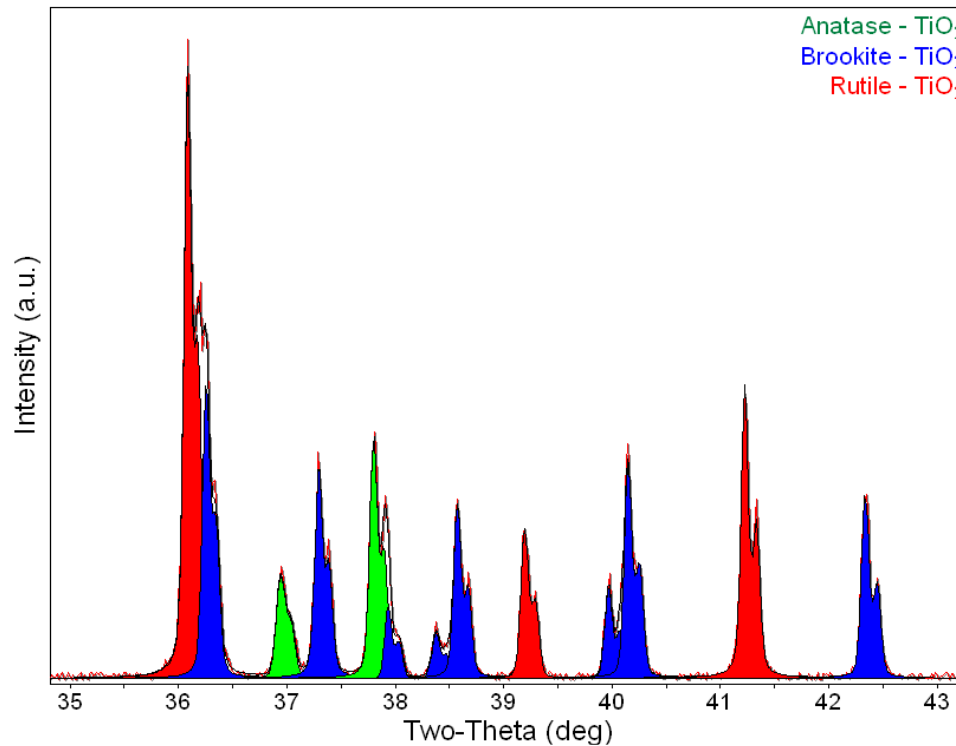
For phase identification you want a random powder (polycrystalline) sample.



Application of Diffraction Data

Phase Analysis

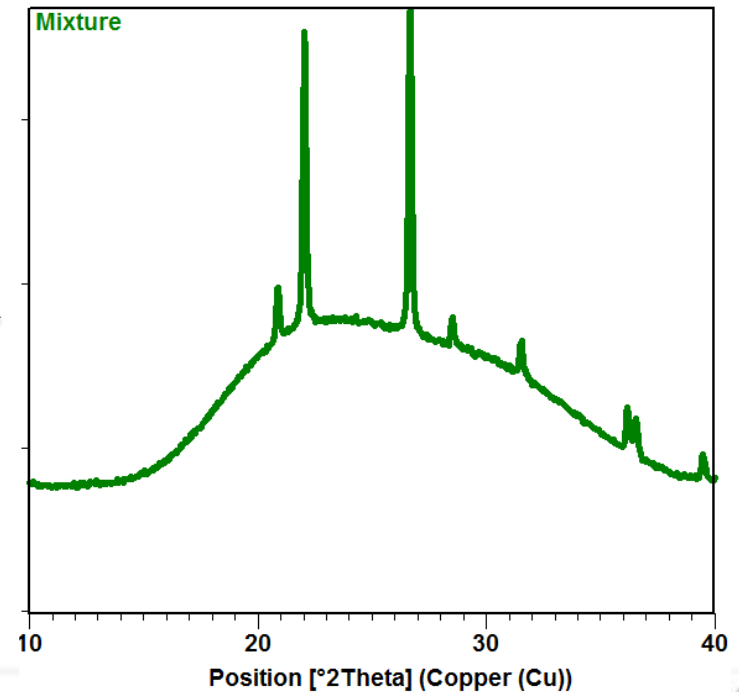
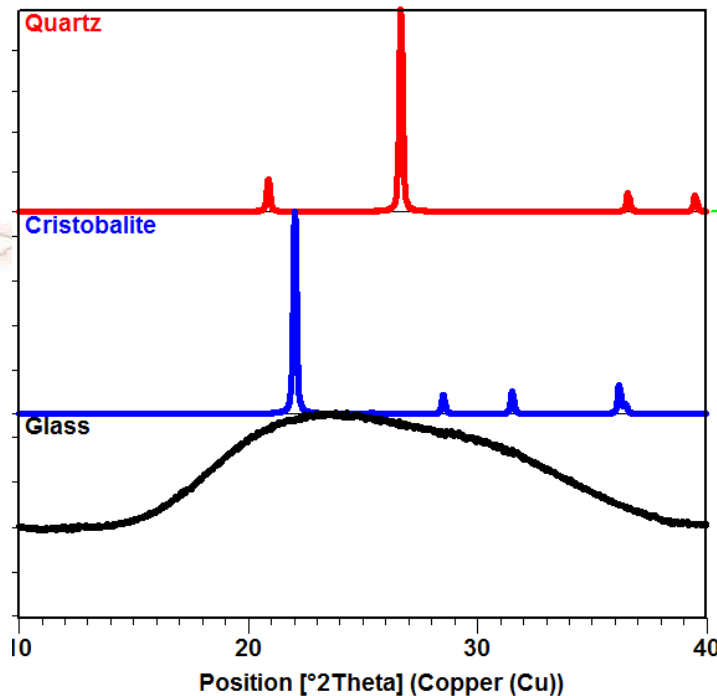
Phases with the same chemical composition can have drastically different diffraction patterns.



Application of Diffraction Data

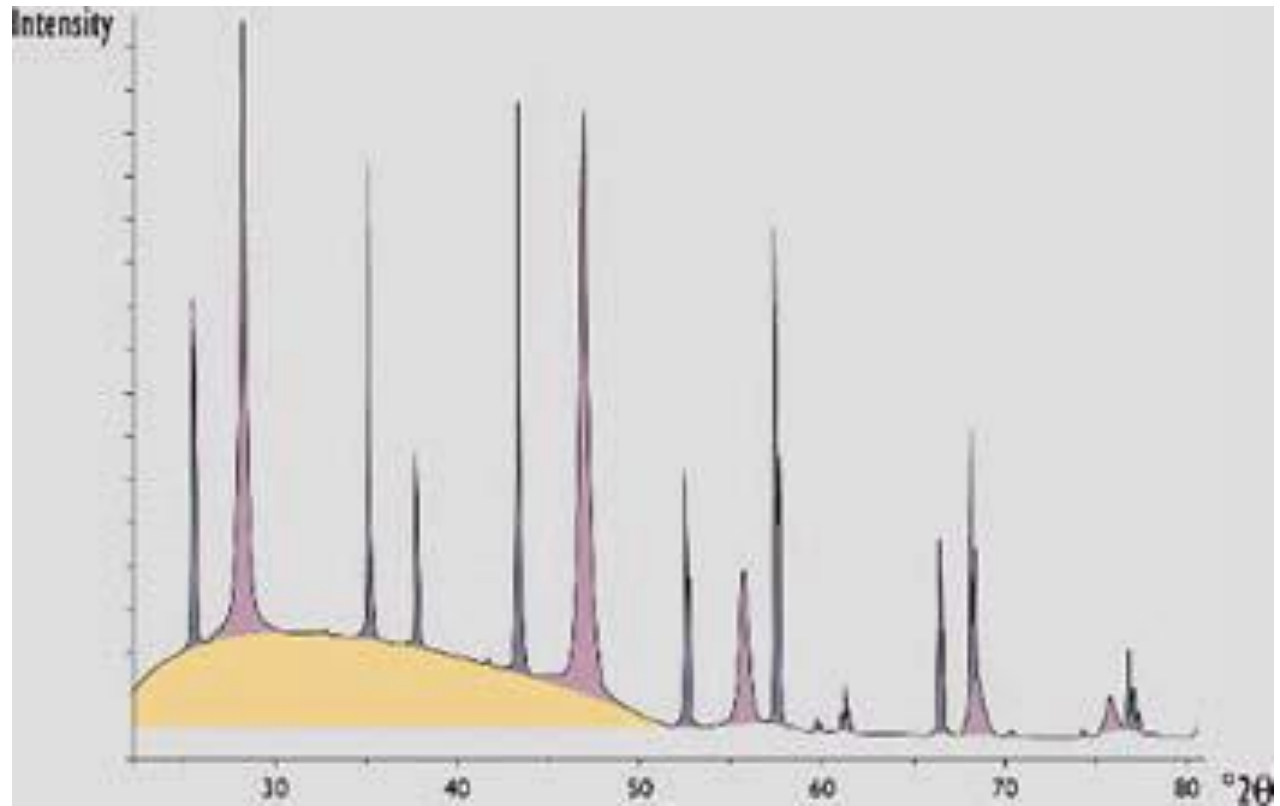
Phase Analysis

The diffraction pattern of a mixture is a simple sum of the scattering from each component phase.



Diffraction Theory

Diffractometer (Powder) Method



Application of Diffraction Data

What determines the possible directions, i.e. angles or 2θ in which a crystal will diffract a beam of x-rays?

Can combine Bragg's law with the plane - spacing equation.

Application of Diffraction Data

For a cubic structure

$$d_{hkl} = \sqrt{\frac{a^2}{h^2 + k^2 + l^2}}$$

Application of Diffraction Data

Example. For a cubic crystal: (like for your homework)

$$n\lambda = 2d\sin\theta$$

Bragg's law

$$\frac{1}{d^2} = \frac{h^2 + k^2 + l^2}{a^2}$$

$$\sin^2 \theta = \frac{\lambda^2}{4a^2} (h^2 + k^2 + l^2)$$

Application of Diffraction Data

Example. For a cubic crystal:

For the 110 plane:

$$\sin^2 \theta = \frac{\lambda^2}{4a^2} (h^2 + k^2 + l^2)$$

$$\sin^2 \theta_{110} = \frac{\lambda^2}{4a^2} (1^2 + 1^2 + 0^2) = \frac{\lambda^2}{4a^2} (2) = \frac{\lambda^2}{2a^2}$$

Application of Diffraction Data

For the 110 plane:

$$\sin^2 \theta_{110} = \frac{\lambda^2}{4a^2} (1^2 + 1^2 + 0^2) = \frac{\lambda^2}{4a^2} (2) = \frac{\lambda^2}{2a^2}$$

$$\lambda = 1.54056 \text{ \AA}$$

$$\sin^2 \theta_{110} = \frac{(0.154056 \text{ nm})^2}{2a^2}$$

Application of Diffraction Data

From your Lab 2 we know that for Chromium $a = 0.2883 \text{ nm}$

So,

$$\sin^2 \theta_{110} = \frac{(0.154056 \text{ nm})^2}{2(0.2883 \text{ nm})^2} = 0.14277$$

$$\sin \theta_{110} = 0.377849$$

$$\theta_{110} = 22.20$$

$$2\theta_{110} = 44.40$$

Application of Diffraction Data

Diffraction Methods

Lab 2: Solving a Cubic system

Crystal Structure Determination

| | | |
|------------|----------------|---------------|
| Al | fcc | 0.4049 |
| Cr | bcc | 0.2883 |
| Cu | fcc | 0.3615 |
| Fe | bcc | 0.2866 |
| Ni | fcc | 0.3523 |
| Si | diamond | 0.5430 |
| TiN | fcc | 0.4241 |

Application of Diffraction Data

Lab 2: Solving a Cubic system

| Bravais Lattice | Allowed Reflections |
|-----------------|---|
| SC | All |
| BCC | $(h + k + l)$ even |
| FCC | h, k and l unmixed |
| DC | h, k and l are all odd <i>Or</i> all are even $(h + k + l)$ divisible by 4 |

Application of Diffraction Data

Lab 2: Solving a Cubic system

The ratio of $(h^2 + k^2 + l^2)$ derived from extinction rules

| | | | | | | | | |
|-----|---|---|----|----|-----|-----|---|-----|
| SC | 1 | 2 | 3 | 4 | 5 | 6 | 8 | ... |
| BCC | 1 | 2 | 3 | 4 | 5 | 6 | 7 | ... |
| FCC | 3 | 4 | 8 | 11 | 12 | ... | | |
| DC | 3 | 8 | 11 | 16 | ... | | | |

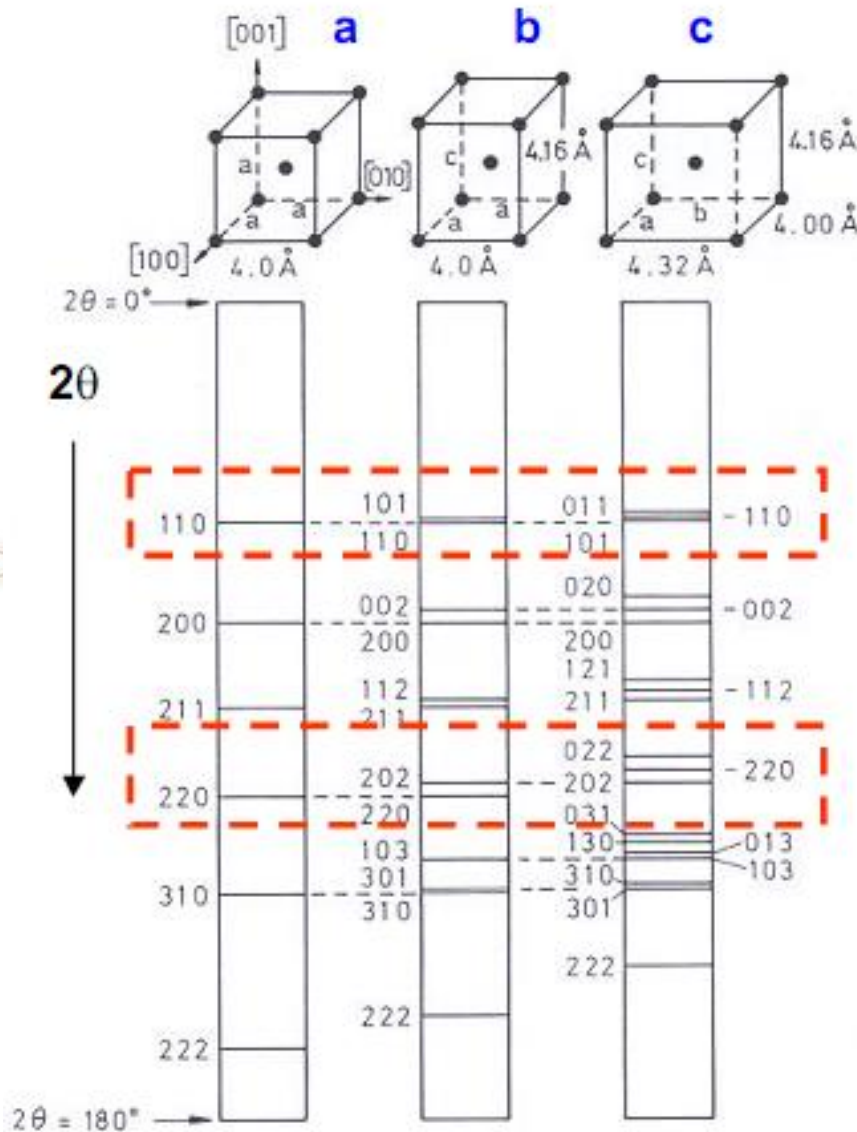
Application of Diffraction Data

For cubic structures it is often possible to distinguish crystal structures by considering the periodicity of the observed reflections.

| $h^2+k^2+l^2$ | 1 | 2 | 3 | 4 | 5 | 6 | 8 | 9 | 10 | 11 | 12 | 13 | 14 | 16 | 17 | 18 | 19 | 20 |
|---------------|-----|-----|-----|-----|-----|-----|-----|----------|-----|-----|-----|-----|-----|-----|----------|----------|-----|-----|
| hkl | 100 | 110 | 111 | 200 | 210 | 211 | 220 | 300, 221 | 310 | 311 | 222 | 320 | 321 | 400 | 410, 322 | 411, 330 | 331 | 420 |
| Simple Cubic | ✓ | ✓ | ✓ | ✓ | ✓ | ✓ | ✓ | ✓ | ✓ | ✓ | ✓ | ✓ | ✓ | ✓ | ✓ | ✓ | ✓ | ✓ |
| BCC | | ✓ | | ✓ | | ✓ | | ✓ | | ✓ | | ✓ | | ✓ | | ✓ | | ✓ |
| FCC | ✓ | | ✓ | | ✓ | | ✓ | | ✓ | | ✓ | | ✓ | | ✓ | | ✓ | |
| Diamond Cubic | ✓ | | ✓ | | ✓ | | ✓ | | ✓ | | ✓ | | ✓ | | ✓ | | ✓ | |

Schematic comparison of XRD results from materials with differing CUBIC crystal structures

Identifying Non-Cubic Phases



- Effect of Symmetry on XRD Pattern

- a. Cubic
 $a=b=c$, (a)
- b. Tetragonal
 $a=b \neq c$ (a and c)
- c. Orthorhombic
 $a \neq b \neq c$ (a, b and c)

- Number of reflections
- Peak position
- Peak splitting

Application of Diffraction Data

Phase Analysis

Qualitative

ID phases by comparison with standard patterns. Estimate of proportions of phases by comparing peak intensities attributed to the identified phases with standard intensity ratios.

Quantitative

Determination of amounts of different phases in multi-phase samples based on precise determination of diffraction intensity and/or determination of the fit of the pattern of each phase to the characteristics of that phase (i.e., amount, crystal structure, crystallite size and shape).

Application of Diffraction Data

Quantitative Phase Analysis

Can be difficult – need to do a complete calibration of instrument, careful prepping of standards, and repetitive measurements.

For quantitative analysis, must equate a concentration of a given phase or phases with line intensities.

Line intensities are affected by a variety of factors.

Table 13.1. Factors Affecting X-ray Powder Diffraction in Line Intensities

| Factor | Parameter |
|---------------------------------|--|
| 1. Structure-sensitive | Atomic scattering factor Structure factor Polarization Multiplicity Temperature |
| 2. Instrument-sensitive | Source intensity |
| (a) <i>Absolute intensities</i> | Diffractometer efficiency Voltage drift Takeoff angle of tube Receiving slit width Axial divergence allowed |
| (b) <i>Relative intensities</i> | Divergence slit aperture Detector dead time |
| 3. Sample-sensitive | Microabsorption Crystallite size Degree of crystallinity Residual stress Degree of peak overlap Particle orientation |
| 4. Measurement-sensitive | Method of peak area measurement Degree of peak overlap Method of background subtraction $K\alpha_2$ stripping or not Degree of data smoothing employed |

Application of Diffraction Data

The intensity equation (from lecture 7, ex: structure factor, multiplicity, Lorenz-polarization factor, temperature factor, absorption factor) describes the dependence of intensity of the diffraction line for a phase α . The entire equation shown here can be reduced, since the 1st and 2nd terms in brackets are constant for the particular setup.

$$I_{(hkl)\alpha} = \left[\frac{I_o \lambda^3}{64\pi r} \left(\frac{e^2}{m_e c^2} \right)^2 \right] \left[\frac{M_{hkl}}{V_\alpha^2} |F_{(hkl)\alpha}|^2 \left(\frac{1 + \cos^2 2\theta \cos^2 2\theta_m}{\sin^2 \theta \cos \theta} \right) \right] \left[\frac{X_\alpha}{\rho_\alpha (\mu/\rho)_s} \right]$$

$I_{(hkl)\alpha}$ = Intensity of reflection of (hkl) in phase α

r = distance from specimen to detector

2nd term = square of classical electron radius

I_o = incident beam intensity

λ = X-ray wavelength

M_{hkl} = multiplicity of reflection hkl of phase α

Next to last term on right = Lorenz-polarization (and monochromator) correction for (hkl)

In that term, $2\theta_m$ = diffraction angle of the monochromator

V_α = volume of the unit cell of phase α

$F_{(hkl)\alpha}$ = structure factor for reflection hkl of phase α

Application of Diffraction Data

The intensity equation (from lecture 7, ex: structure factor, multiplicity, Lorenz-polarization factor, temperature factor, absorption factor) describes the dependence of intensity of the diffraction line for a phase α . The entire equation shown here can be reduced, since the 1st and 2nd terms in brackets are constant for the particular setup.

$$I_{(hkl)\alpha} = \left[\frac{I_o \lambda^3}{64\pi r} \left(\frac{e^2}{m_e c^2} \right)^2 \right] \left[\frac{M_{hkl}}{V_\alpha^2} |F_{(hkl)\alpha}|^2 \left(\frac{1 + \cos^2 2\theta \cos^2 2\theta_m}{\sin^2 \theta \cos \theta} \right) \right] \left[\frac{X_\alpha}{\rho_\alpha (\mu/\rho)_s} \right]$$

X_α – weight fraction of α

ρ_α – density of phase α

$(\mu/\rho)_s$ – mass attenuation coefficient of sample.

Application of Diffraction Data

Quantitative Phase Analysis

Therefore the total adsorption of the sample is a sum of the products of the individual attenuation coefficients and weight factions (two unknowns)

So need to use various methods to solve equation.

Methods

- absorption-diffraction
- standard additions
- internal standards



Quantitative Phase Analysis

Absorption-Diffraction Method

$$\frac{I_{(hkl)\alpha}}{I_{(hkl)\alpha}^o} = \frac{(\mu / \rho)_{\alpha}}{(\mu / \rho)_s} X_{\alpha}$$

where

$I_{(hkl)\alpha}$ – intensity of phase α of unknown

$I_{(hkl)\alpha}^o$ – intensity of pure sample of phase α

Application of Diffraction Data

Quantitative Phase Analysis

For a binary mixture:

$$\frac{I_{(hkl)\alpha}}{I_{(hkl)\alpha}^o} = \frac{X_{\alpha}(\mu/\rho)_{\alpha}}{X_{\alpha}(\mu/\rho)_{\alpha} + X_{\beta}(\mu/\rho)_{\beta}}$$

Since $X_{\alpha} + X_{\beta} = 1$, can simplify equation to the Klug equation:

$$X_{\alpha} = \frac{(I_{(hkl)\alpha} / I_{(hkl)\alpha}^o)(\mu/\rho)_{\beta}}{(\mu/\rho)_{\alpha} - (I_{(hkl)\alpha} / I_{(hkl)\alpha}^o)[(\mu/\rho)_{\alpha} - (\mu/\rho)_{\beta}]}$$

Application of Diffraction Data

Quantitative Phase Analysis

$$X_{\alpha} = \frac{(I_{(hkl)\alpha} / I_{(hkl)\alpha}^{\circ})(\mu / \rho)_{\beta}}{(\mu / \rho)_{\alpha} - (I_{(hkl)\alpha} / I_{(hkl)\alpha}^{\circ})[(\mu / \rho)_{\alpha} - (\mu / \rho)_{\beta}]}$$

Example: SiO₂ in SiO₂/CaSiO₃

$(\mu/\rho)_{\alpha}$ for SiO₂ is 35.9 and $(\mu/\rho)_{\beta}$ for CaSiO₃ is 74.1

I for SiO₂ phase is 4270 counts and I for pure SiO₂ is 10,000 counts

then
$$X_{\alpha} = \frac{0.427 \times 74.1}{35.9 - (0.427 \times (35.9 - 74.1))} = 60.6\%$$

Application of Diffraction Data

Quantitative Phase Analysis

Standard Addition Method or “spiking” method

Method used to determine α phase in a mixture, as long as one other phase, β , has a diffraction line that does not overlap with any α line.

β does not even have to be identified.

Application of Diffraction Data

Quantitative Phase Analysis

With this method, some of the pure α phase is added to the mixture containing the unknown concentration of α .

$$\frac{I_{(hkl)\alpha}}{I_{(hkl)'\beta}} = K(X_{\alpha} + Y_{\alpha})$$

where

X_{α} is the initial weight fraction of phase α

X_{β} is the initial weight fraction of phase β

Y_{α} is the number of grams of pure phase α added per gram of the original sample.

Application of Diffraction Data

Quantitative Phase Analysis

After several additions of Y_α grams of the α phase, a plot of I_α/I_β versus Y_α can be constructed.

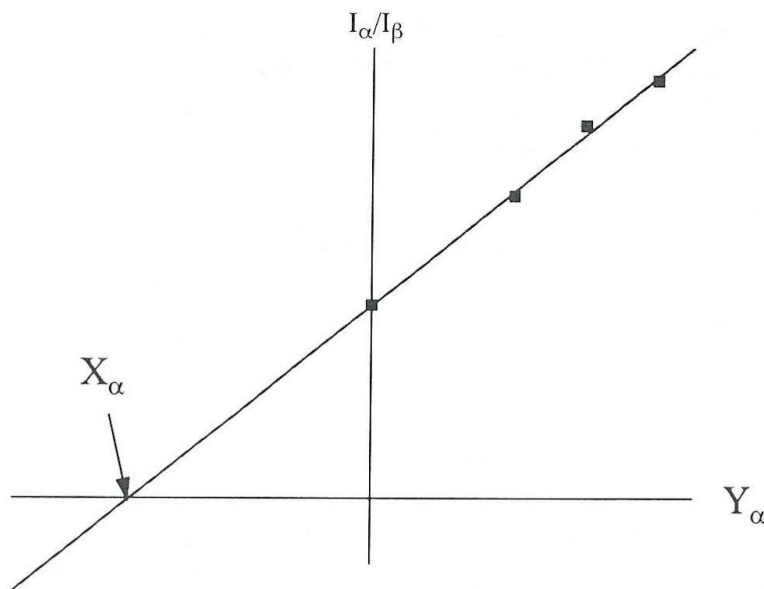


Figure 13.8. Spiking method analysis: plot of the ratio of I_α to the intensity of a reference line as a function of Y_α , the number of grams of α added per gram of sample.

Application of Diffraction Data

Quantitative Phase Analysis

Internal Standard Method

Most common

Plot a calibration curve of $I_{(hkl)\alpha}/I_{(hkl)\beta}$ versus X_α/X_β with k as the slope.

$$\frac{I_{(hkl)\alpha}}{I_{(hkl)\beta}} = k \frac{X_\alpha}{X_\beta}$$

Application of Diffraction Data

Quantitative Phase Analysis

In this method, a known amount, X_{β} , of an internal standard is added to a mixture of phases.

The addition of this new phase increases the complexity of the pattern, so must be careful in choosing the standard.

Usually, F-centered cubic materials with small unit cells are used because of their simple patterns.

Application of Diffraction Data

Quantitative Phase Analysis

Rietveld Method

Quantitative method based on the use of the total pattern.

Involves fitting the entire diffraction pattern with a synthetic diffraction pattern, which is either a produced or calculated standard pattern.

Rietveld refinement is conducted by minimizing the sum of the weighted, squared differences between observed and calculated intensities at each step.

Application of Diffraction Data

Quantitative Phase Analysis

The full-pattern approach pioneered by Dr. Hugo M. Rietveld attempts to account for all of the contributions to the diffraction pattern to discern all of the component parts by means of a least-squares fit of the diffraction pattern.

The method is made possible by the power of digital data processing and very complicated software.

Input data needed includes space group symmetry, atomic positions, site occupancies, lattice parameters for each phase, profile shape, a background function, and a scale factor.

Can set certain data and let others vary, i.e. scale factor, profile, background, and lattice parameter.

Application of Diffraction Data

Quantitative Phase Analysis

Rietveld Method

Quantitative method based on the use of the total pattern.

The method is made possible by the power of digital data processing and very complicated software

Originally conceived only for use with extremely clean neutron diffraction data, the method has evolved to deal with the relatively poor-quality of data from conventionally-sourced diffractometers.

Rietveld refinement is conducted by minimizing the sum of the weighted, squared differences between observed and calculated intensities at each step.

Quantitative Methods

Rietveld Method

The method is capable of much greater accuracy in quantifying XRD data than any peak-intensity-based method because of the systemic “whole-pattern” approach

The initial primary use of the method was (and still is) to make precise refinements of crystal structures based on fitting the experimental diffraction pattern to precise structure

Though it generally has a fairly steep learning curve, very sophisticated software is available at no cost to do the refinements: Major packages include GSAS and FullPROF

Reitveld's 1969 paper is recommended for further reading

<http://crystal.tau.ac.il/xtal/paper2/paper2.html>

Quantitative Methods

FULLPAT: A Full Pattern Quant System

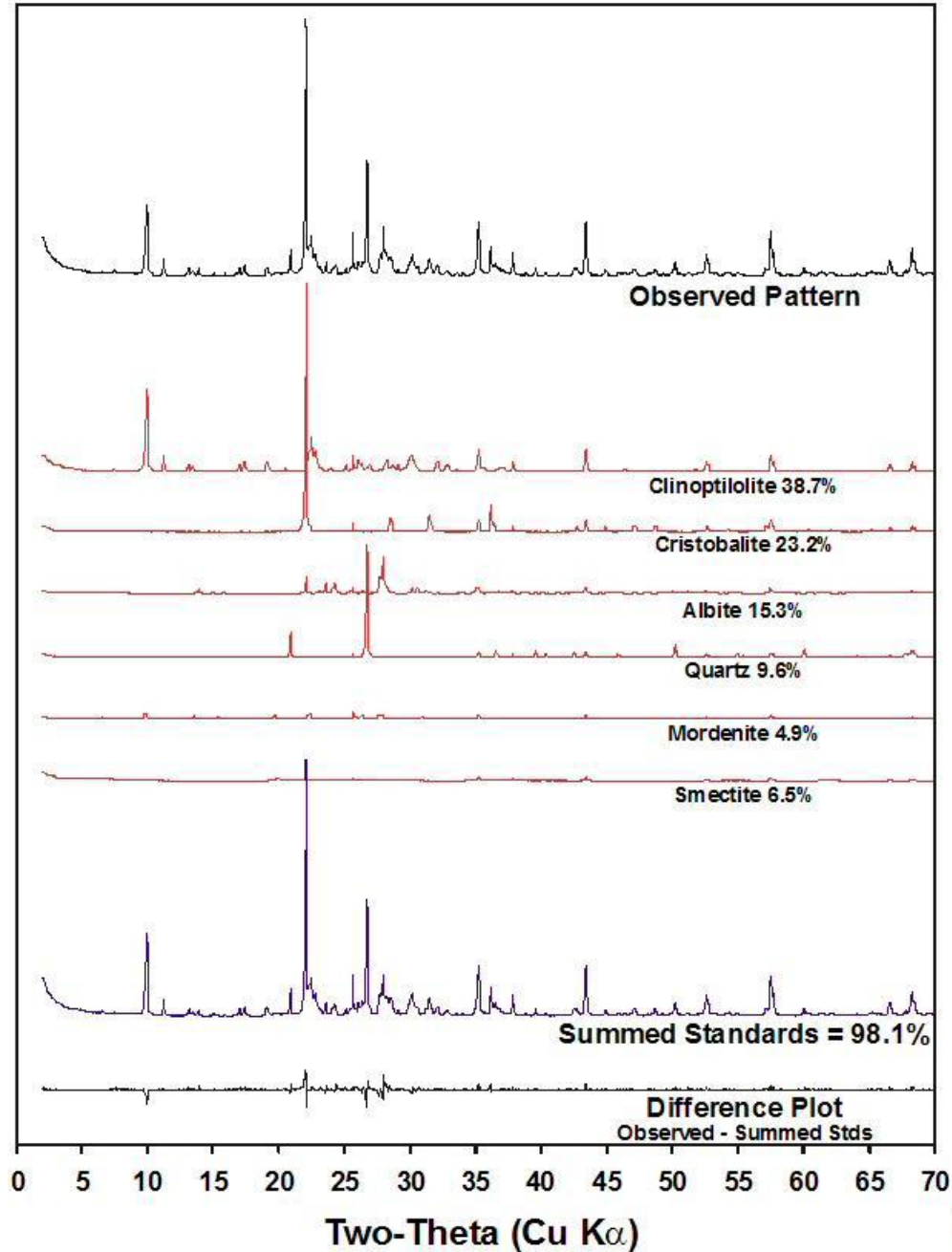
Developed by Steve Chipera and Dave Bishat LANL (primarily for use in analysis of Yucca Mountain Tuff samples).

Is a full pattern fitting system but (unlike Reitveld) does not do detailed structure determination.

Uses the built-in Solver functions of Microsoft Excel. Will work on virtually any computer that has MS Excel on it (as long as the correct extensions are installed).

Software is free and in the public domain (your tax dollars at work); available on <ftp://eps.unm.edu/pub/xrd>

Basically, the program makes use of the fact that the total diffraction pattern is the sum of the diffraction patterns of the constituent phases, and does a least-squares fit on the observed (sample) pattern to the appropriate standard patterns.



Application Example

Effect of electrochemical deposition parameters

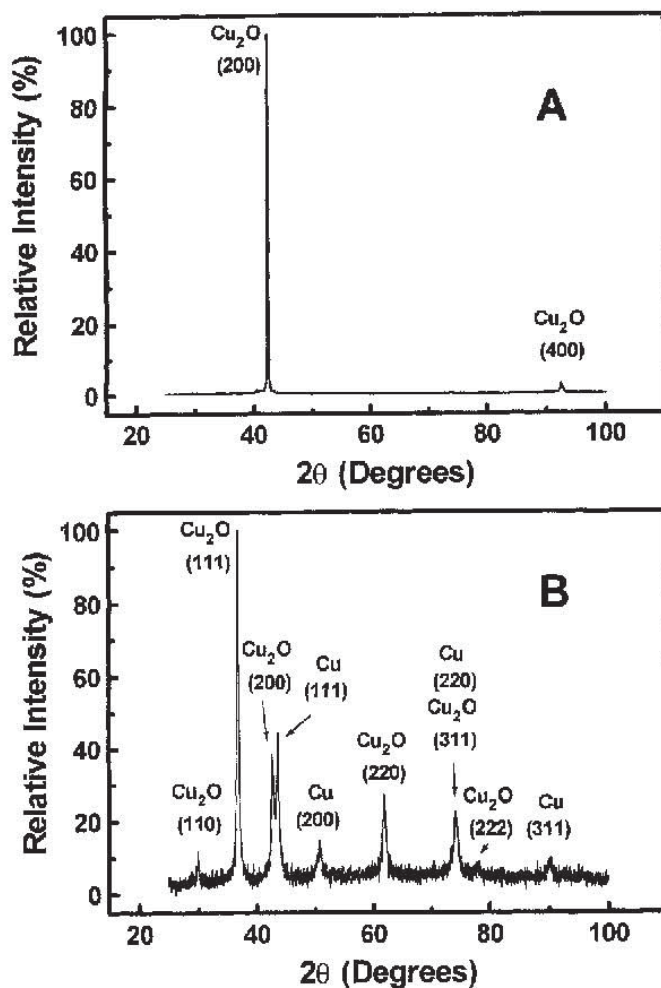


Fig. 2. Comparison of the X-ray diffraction (XRD) patterns of a pure Cu_2O film (A) deposited at 0.05 mA/cm^2 and a $\text{Cu/Cu}_2\text{O}$ nanocomposite film (B) deposited at 0.5 mA/cm^2 . The Cu_2O film has a strong [100] orientation and large crystallite sizes, while the $\text{Cu/Cu}_2\text{O}$ film is randomly oriented. The crystallite radii of Cu and Cu_2O are estimated to be 6 and 12 nm, respectively. The phase composition of the nanocomposite is 50 mol-% Cu and 50 mol-% Cu_2O . Films were deposited onto 1.5 cm^2 polycrystalline Pt substrates.

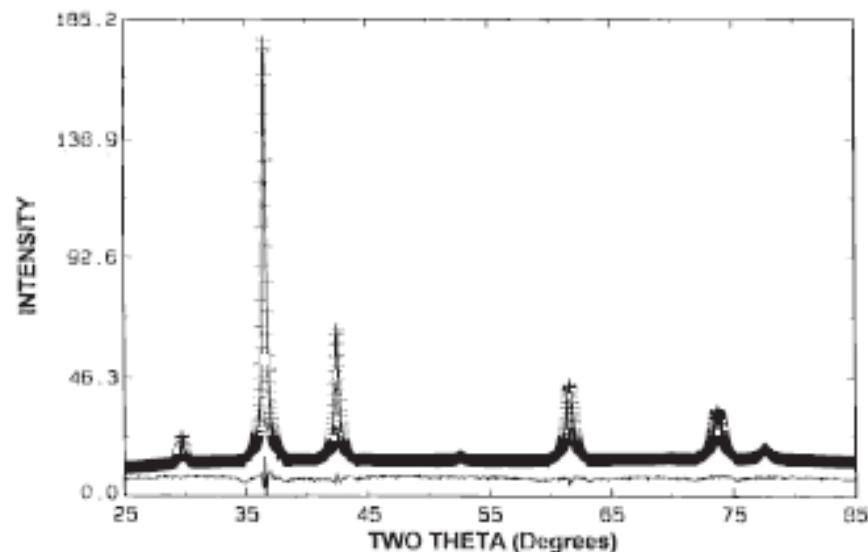


Figure 5. Rietveld analysis for powder produced by grinding several films deposited at $65 \text{ }^\circ\text{C}$ and $E = -0.45 \text{ V}$. Powder X-ray data (solid line), Rietveld fit (crosses) and difference pattern (solid line shown below data) are shown for Cu_2O .

Application Example

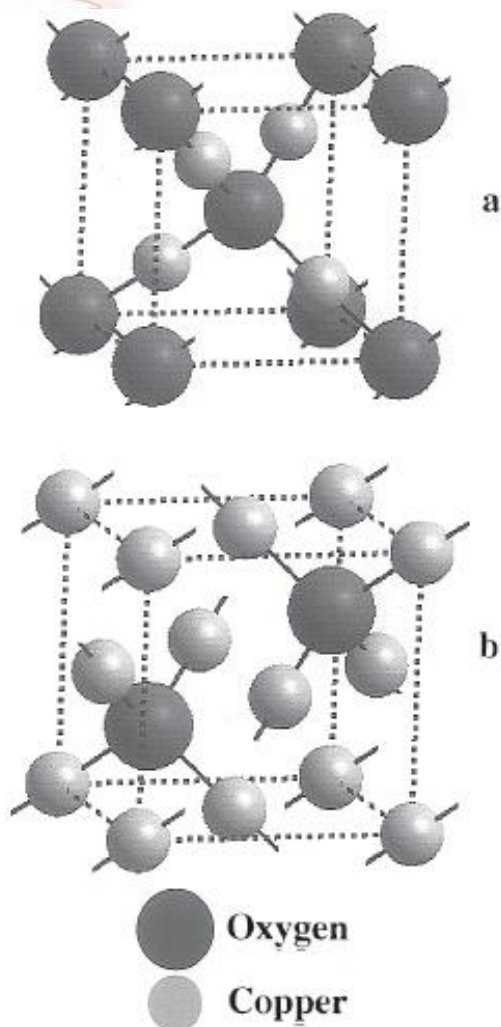


Figure 6. Cuprite structure for Cu_2O . Copper atoms are represented by small light spheres and oxygen atoms are represented by large dark spheres. (a) Copper special positions at $(0.25, 0.25, 0.25)$; $(0.75, 0.75, 0.25)$; $(0.75, 0.25, 0.75)$; $(0.25, 0.75, 0.75)$ and oxygen special positions at $(0, 0, 0)$; $(0.5, 0.5, 0.5)$. (b) Copper special positions at $(0, 0, 0)$; $(0.5, 0.5, 0)$; $(0.5, 0, 0.5)$; $(0, 0.5, 0.5)$ and oxygen special positions at $(0.75, 0.75, 0.75)$; $(0.25, 0.25, 0.25)$.

Table 2. Reflections, d Spacings, and Intensities for the Experimental, Calculated, and JCPDS Card #5-667 for Cu_2O

| reflection (hkl) | obsd d spacing (Å) | obsd intensity I/I_0 (%) | calcd d spacing (Å) | calcd intensity I/I_0 (%) | JCPDS d spacing (Å) | JCPDS intensity I/I_0 (%) |
|-------------------------|----------------------------|----------------------------------|-----------------------------|-----------------------------------|-----------------------------|-----------------------------------|
| 110 | 3.020 | 7 | 3.020 | 6 | 3.020 | 9 |
| 111 | 2.464 | 100 | 2.463 | 100 | 2.465 | 100 |
| 200 | 2.133 | 37 | 2.133 | 36 | 2.135 | 37 |
| 211 | 1.742 | 2 | 1.742 | 1 | 1.743 | 1 |
| 220 | 1.510 | 31 | 1.510 | 31 | 1.510 | 27 |
| 311 | 1.287 | 22 | 1.286 | 25 | 1.287 | 17 |
| 222 | 1.232 | 4 | 1.232 | 5 | 1.233 | 4 |
| 400 | 1.067 | 2 | 1.067 | 3 | 1.067 | 2 |
| 331 | 0.979 | 4 | 0.978 | 5 | 0.979 | 4 |
| 420 | 0.954 | 3 | 0.954 | 3 | 0.954 | 3 |
| 422 | 0.870 | 3 | 0.870 | 4 | 0.871 | 3 |
| 511 | | | | | 0.821 | 3 |

Application Example

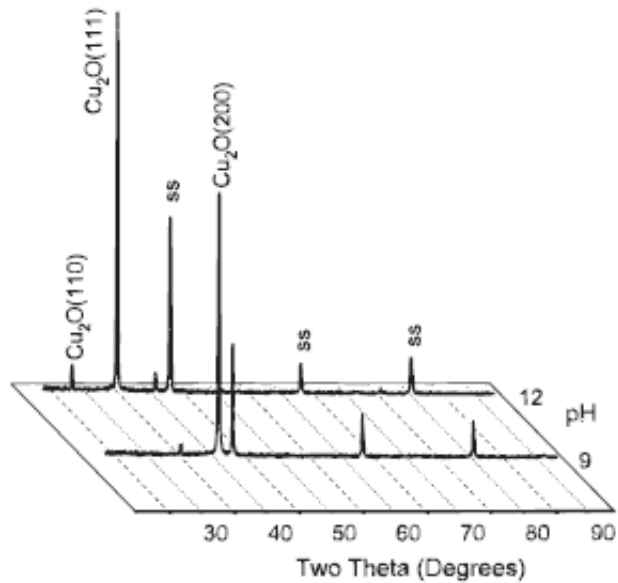


Figure 7. X-ray diffraction patterns of Cu_2O deposited from solutions of pH 9 and 12. The bath temperature is 65 °C and the applied current density is 0.8 mA/cm².

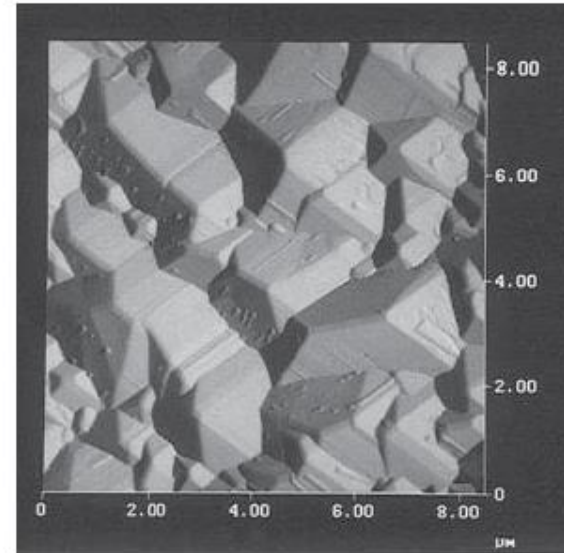


Figure 8. Top-view AFM image of a Cu_2O film deposited at pH 9, $E = -0.45$ V and 65 °C. AFM; z range = 2.5 μm, scan rate = 0.75 Hz.

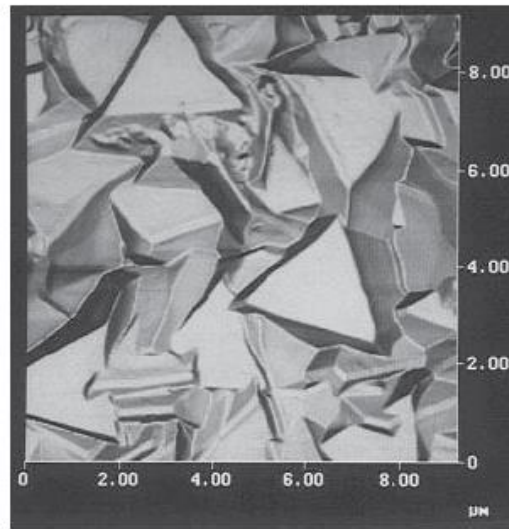


Figure 9. Top-view AFM image of a Cu_2O film deposited at pH 12, $E = -0.45$ V and 65 °C. AFM; z range = 4.2 μm, scan rate = 0.75 Hz.

Application Example

Nucleation and Growth Studies

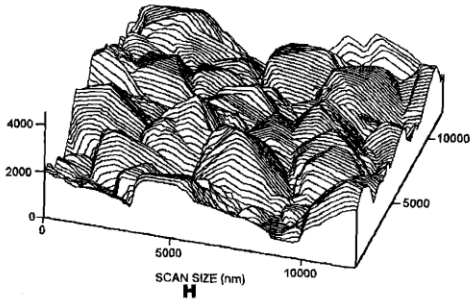
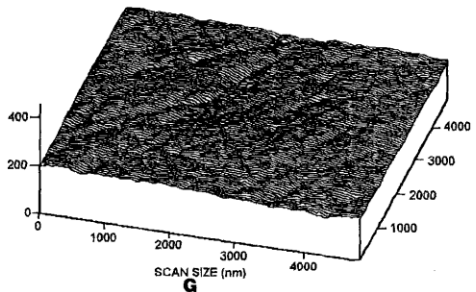
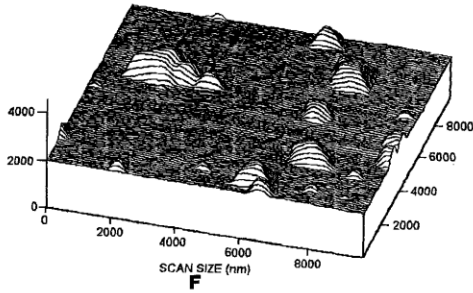
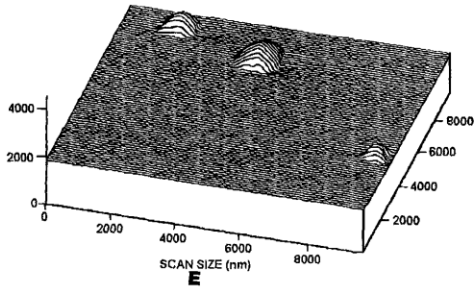
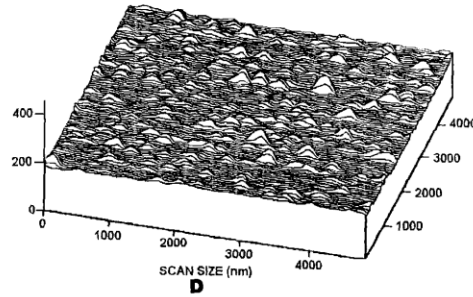
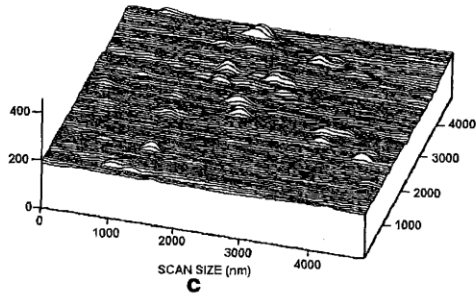
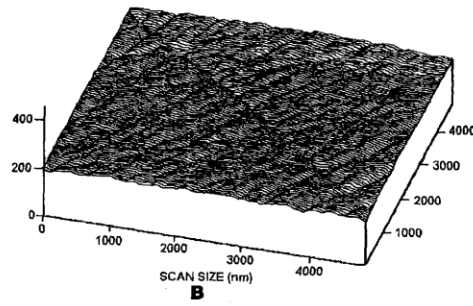
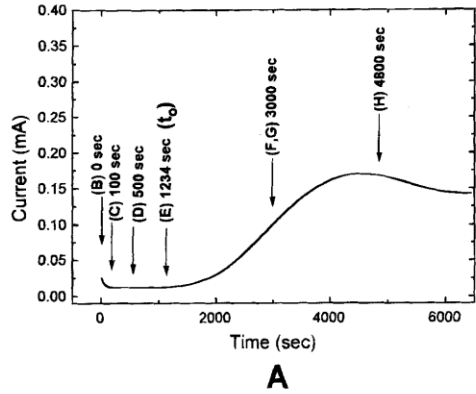


Fig. 12. Atomic force microscopy for several deposition times resulting from a potential step to an overpotential of 149 mV. (A) The location along the current-time transient for (B) 0 s, (C) 100 s, (D) 500 s, (E) 1234 s, (F) 3000 s, (G) 3000 s between nuclei over an amorphous surface and (H) 4800 s.

Application Example

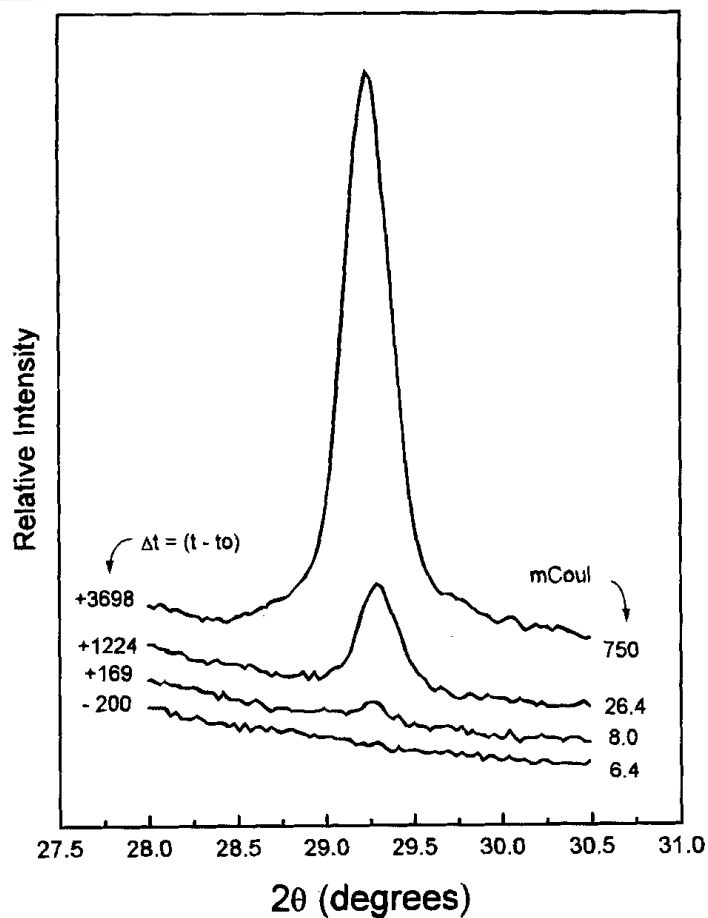


Fig. 10. Low incident angle x-ray diffraction for Ti_2O_3 deposited at an overpotential of 149 mV onto glassy carbon for various deposition times. Crystalline material was observed by diffraction from the (222) planes of Ti_2O_3 after the induction time. Δt represents the deposition time minus the induction time for an overpotential of 149 mV. Positive values of Δt are after the induction time and negative values are before the induction time. The accumulated charge for each trial is shown in millicoulombs on an electrode geometric area of 0.8 cm^2 .

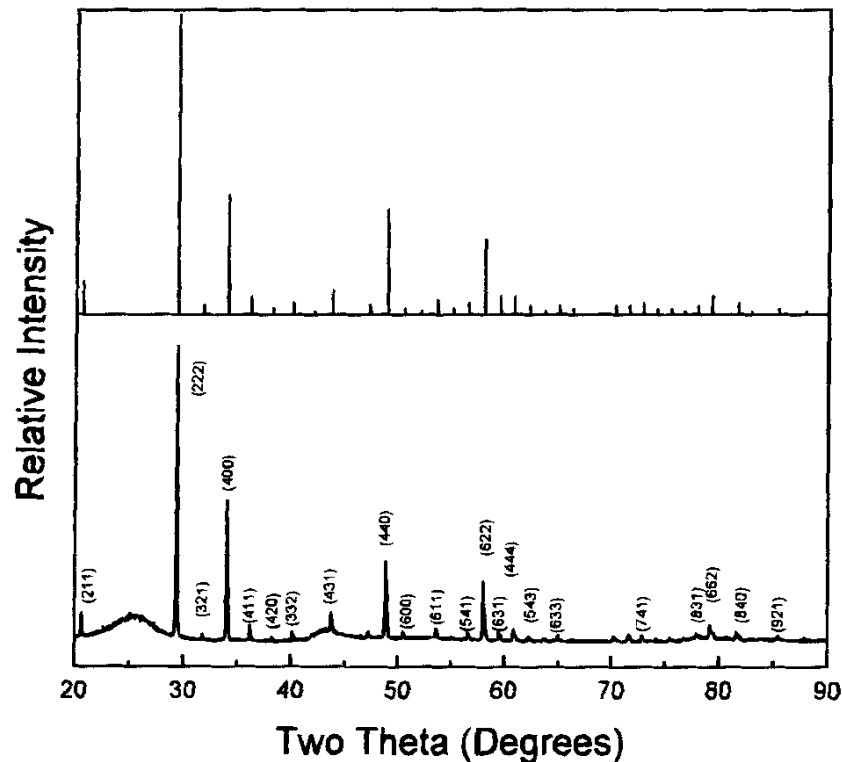
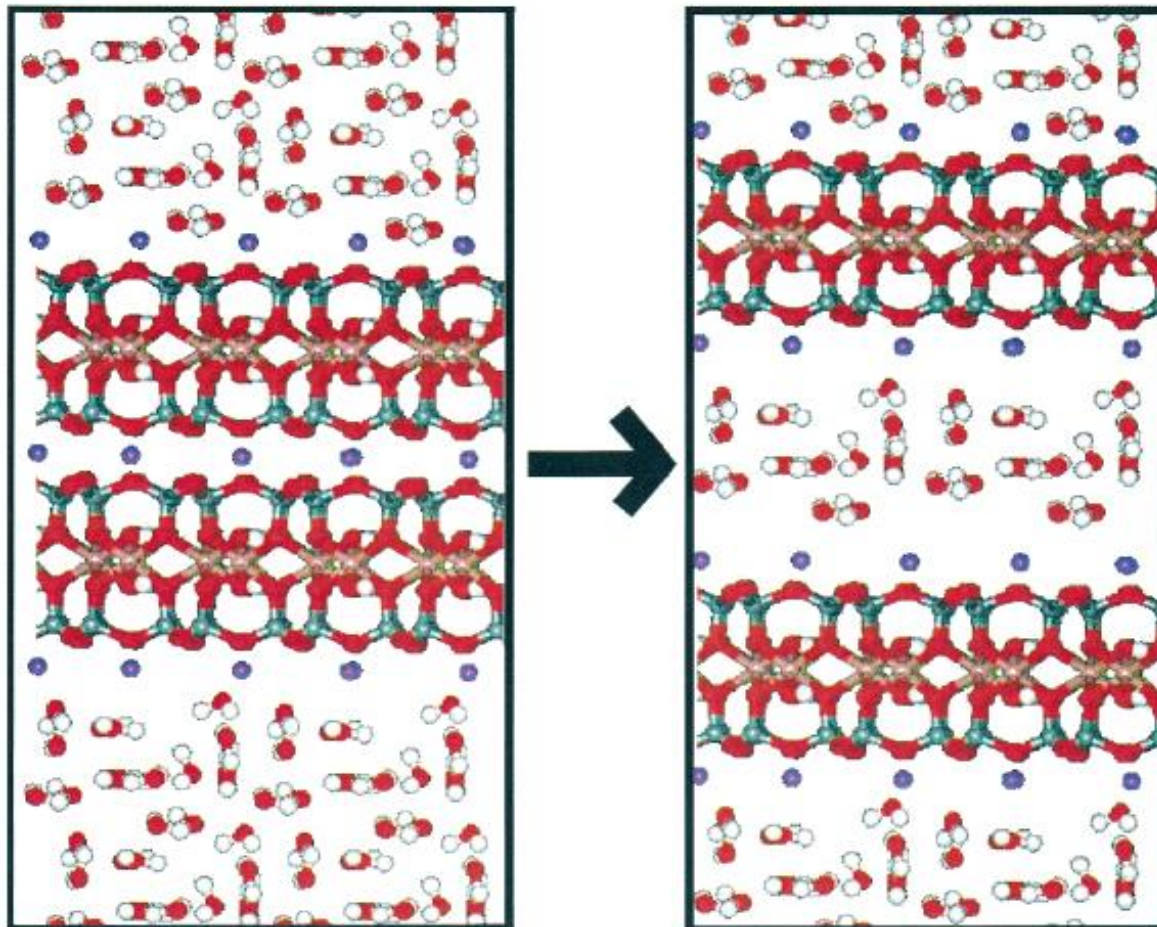


Fig. 15. X-ray diffraction for Ti_2O_3 deposited onto glassy carbon during a potential step from open circuit to an overpotential of 149 mV for a deposition time of 3000 s. The theoretical stick pattern for a random powder is shown in the top section. A comparison of relative intensities between theoretical and experimental indicates that the film is randomly oriented similar to a powder pattern. Experimental patterns were generated in the symmetric scan mode.

Applications



Crystal
and
external
structure

Figure 2. Intercalation scheme of nanoclay mechanics occurring when dissolved platelets (far left) expand their gallery spacing to accommodate intercalants (right). Neutral or cationic species may be intercalated into nanoclay platelets.

Applications

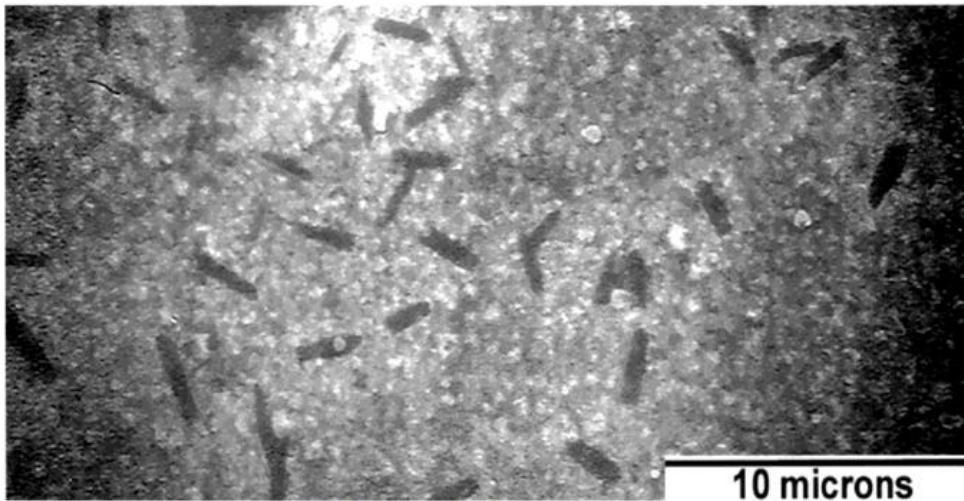


Figure 4. Scanning electron micrograph of a film deposited with a standard electrochemical cell setup at higher stir rates. Montmorillonite layered silicate platelets (dark, rodlike objects) can be seen extruding from the surface of the film.

Ceramic +
Metal

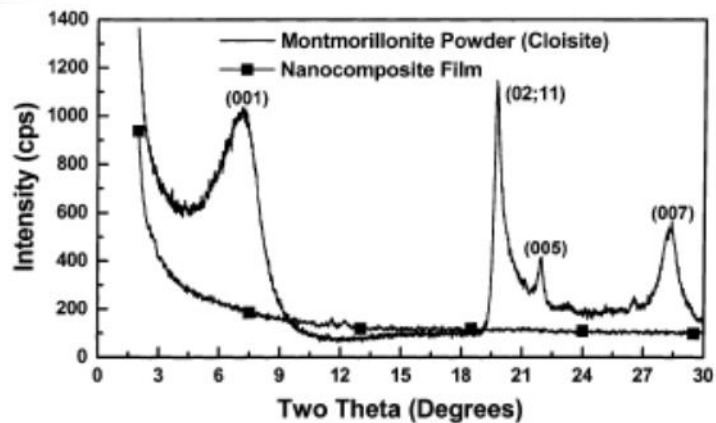
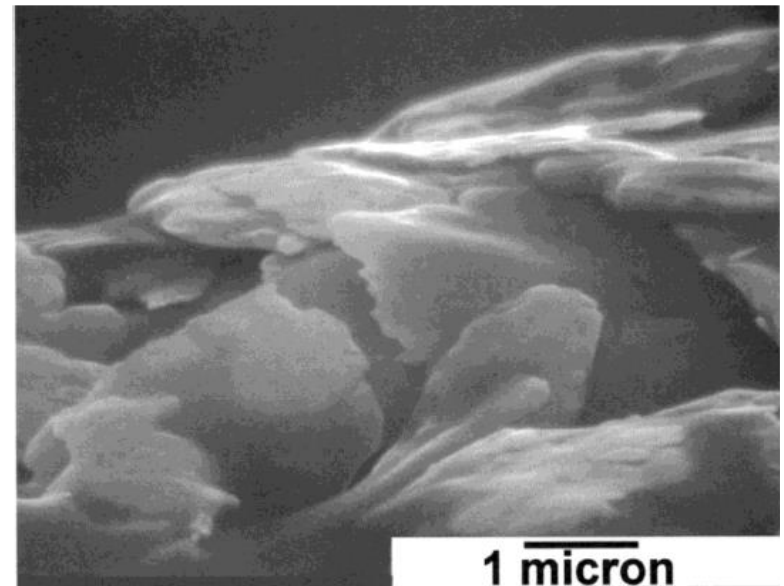


Figure 5. This XRD pattern compares the Ni-MLS film (squares) grown in the third electrochemical cell setup to the pure nanoclay powder (solid line). In the Ni-MLS pattern, the 001 nanoclay peak has disappeared, indicating that the incorporated nanoclay is exfoliated and exists as individual platelets.



Application of Diffraction Data

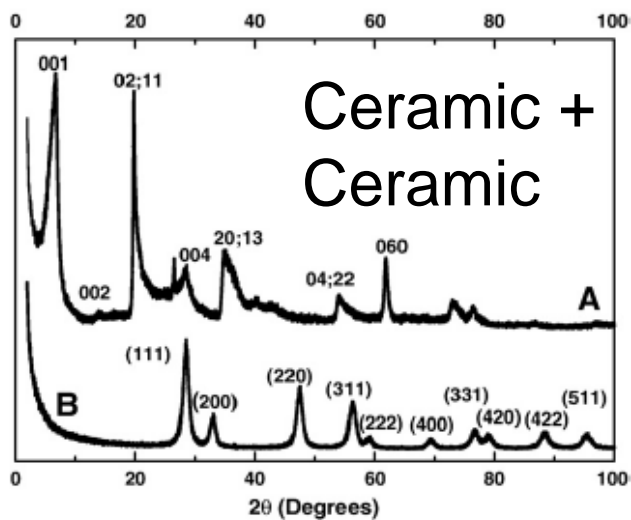


Fig. 1. XRD patterns for montmorillonite (A) and electrogenerated nanocrystalline CeO_2 powder (B). The corresponding phase assignment for CeO_2 is listed in Table 1.

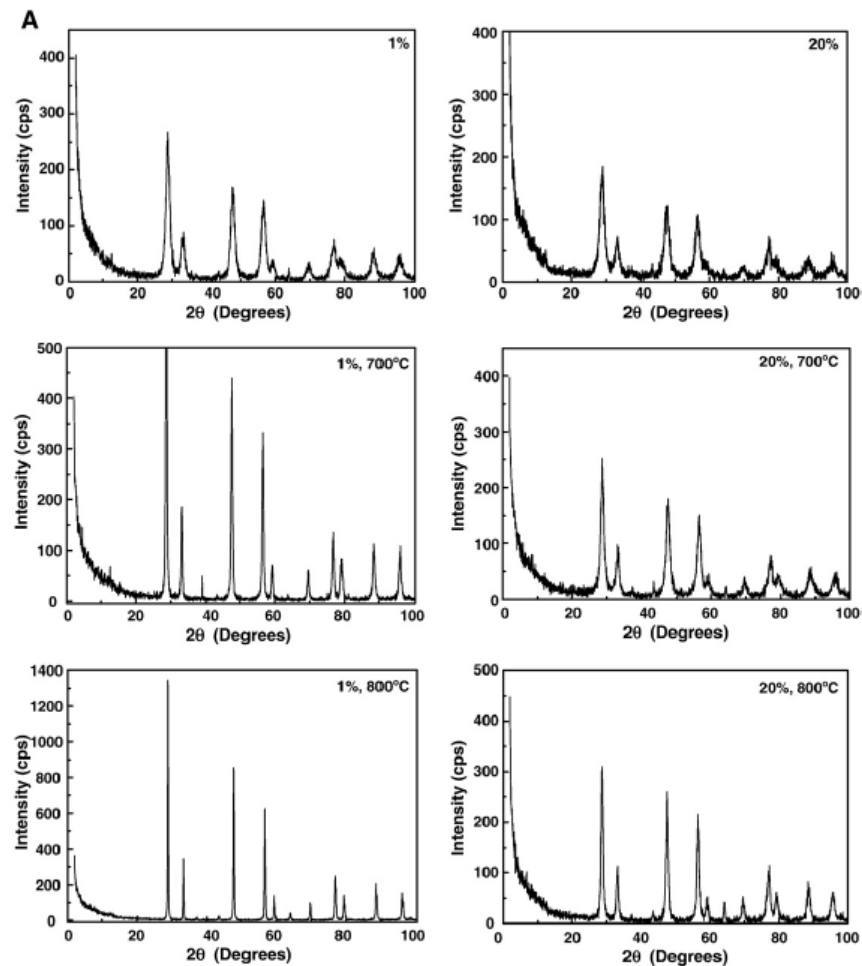


Fig. 5. A and B. XRD patterns for CeO_2 /montmorillonite nanocomposites before and after sintering at 700, 800, 900, 1000, 1100 °C.

Table 1
Comparison between experimental and PDF data for CeO_2

| <i>h k l</i> | Experimental data | | PDF#34-0394 | |
|--------------|-------------------|----------------------------------|-------------|-----------------------|
| | 2θ | <i>I</i> / <i>I</i> ₀ | 2θ | <i>I</i> (<i>f</i>) |
| 111 | 28.48 | 100 | 28.554 | 100 |
| 200 | 33.07 | 30 | 33.081 | 30 |
| 220 | 47.42 | 56 | 47.478 | 52 |
| 311 | 56.29 | 43 | 56.334 | 42 |
| 222 | 59.04 | 10 | 59.085 | 8 |
| 400 | 69.45 | 9 | 69.400 | 8 |
| 331 | 76.64 | 18 | 76.698 | 14 |
| 420 | 78.93 | 13 | 79.067 | 8 |
| 422 | 88.36 | 15 | 88.410 | 14 |
| 511 | 95.32 | 13 | 95.394 | 11 |

Experimental data from Fig. 1.

Ceramic + Ceramic

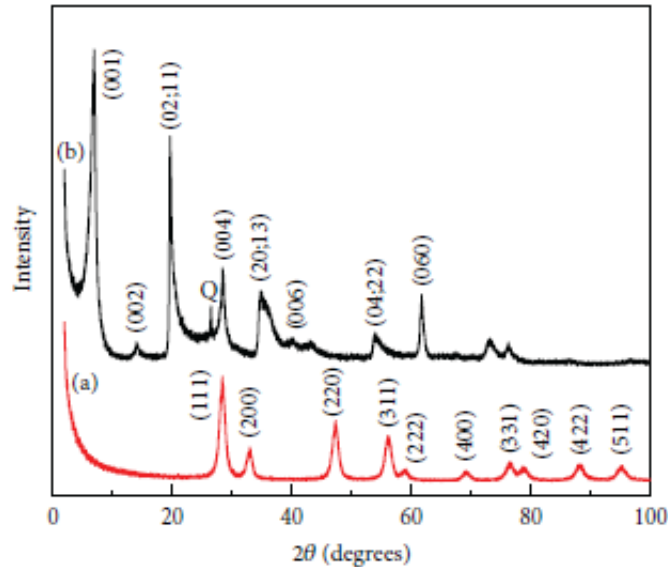


FIGURE 2: X-ray diffraction patterns of (a) CeO₂ powder and (b) Na-montmorillonite powder.



FIGURE 8: Cross-sectional SEM of a CeO₂/MMT nanocomposite electrodeposited film using potentiostatic conditions at $E = 1.10$ V and 25°C (bar represents 10 μm).

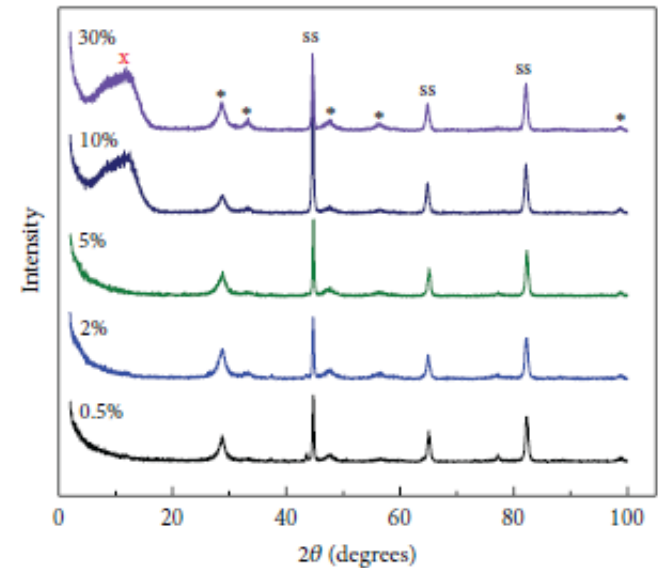


FIGURE 3: X-ray diffraction patterns of CeO₂/MMT nanocomposite films deposited from 0.5, 2, 5, 10, and 30% MMT concentrations in the plating solution (* represents the cerium oxide reflections, and red x represents the 00l reflections for the layered silicate).

Application Example

Medical + Chemistry

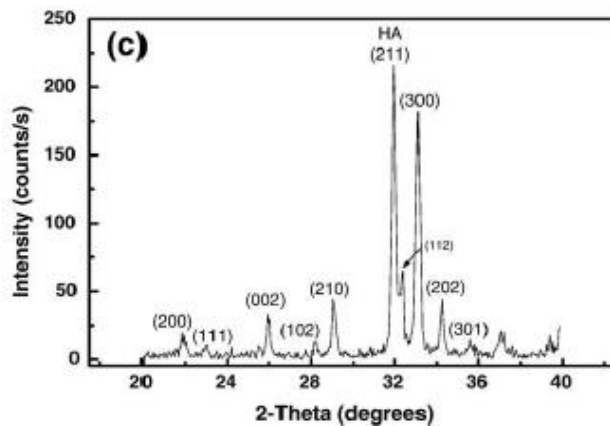
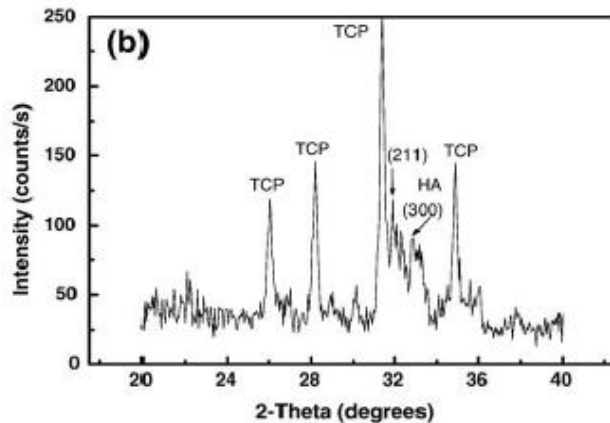
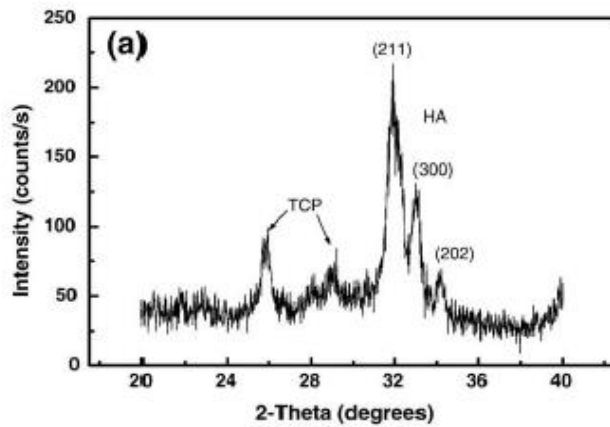


Fig. 2. XRD patterns of electrodeposited HA coatings at $E_{\text{appl}} = -1.3$ V vs SCE and $T = 65$ °C, for 1 h (a) as deposited, (b) sintered for 1 h at 600 °C and (c) vacuum sintered at 800 °C for 1 h.

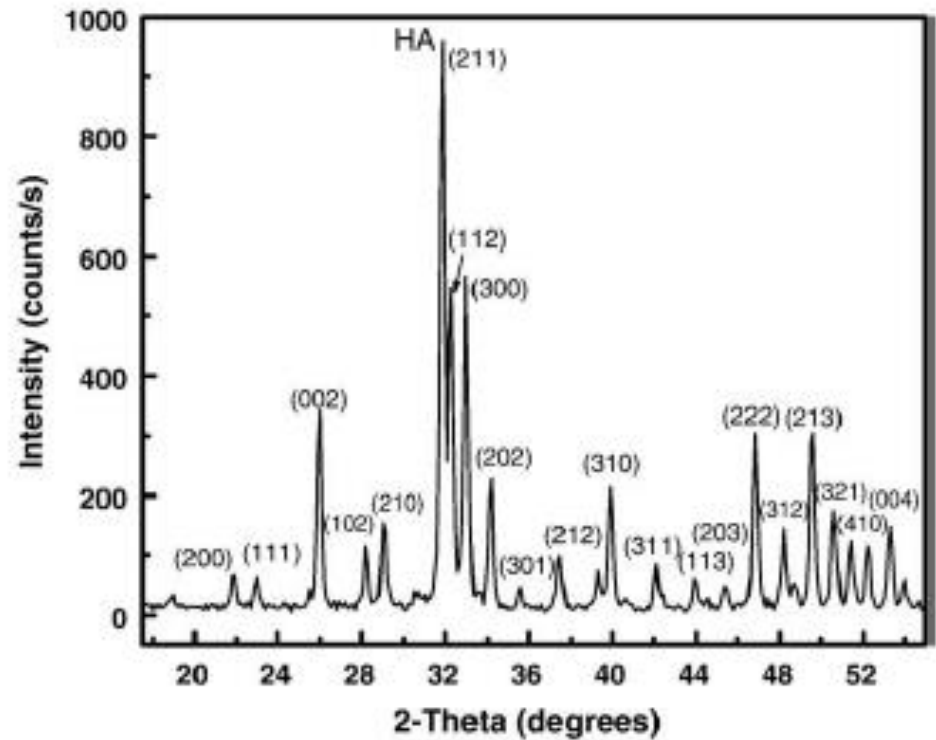
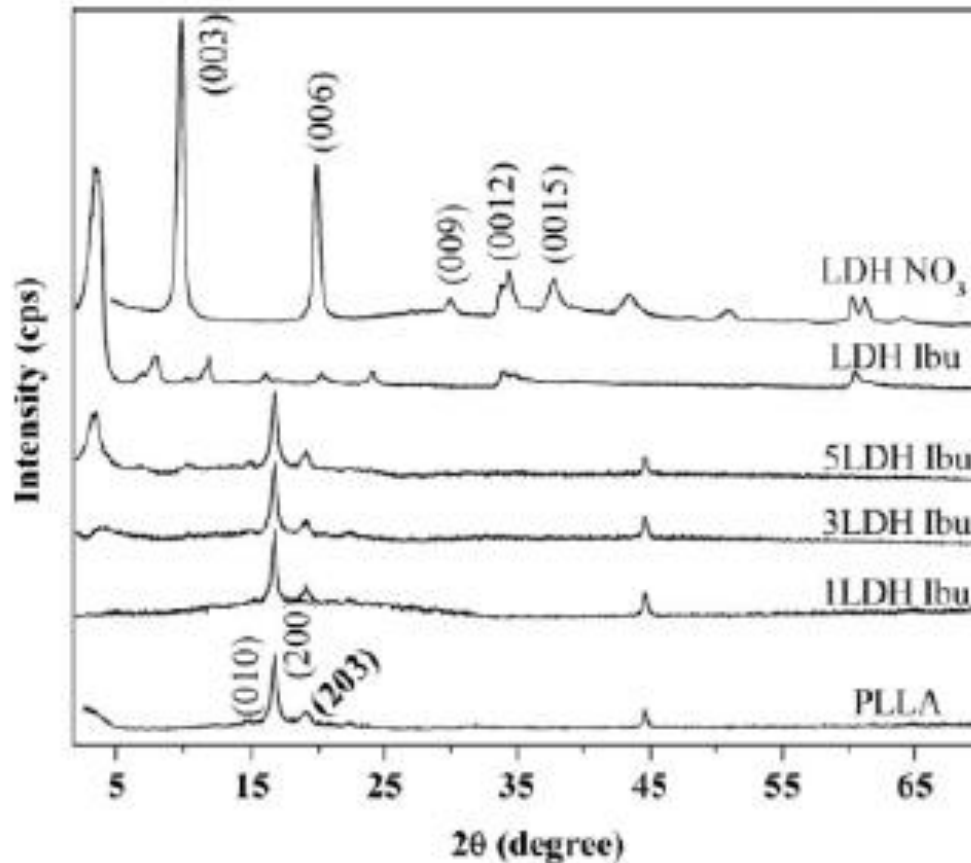


Fig. 6. XRD pattern of electrodeposited double-layer HA coating at $E_{\text{appl}} = -1.3$ V vs SCE and $T = 65$ °C for 1 h sintered at 600 °C in air.

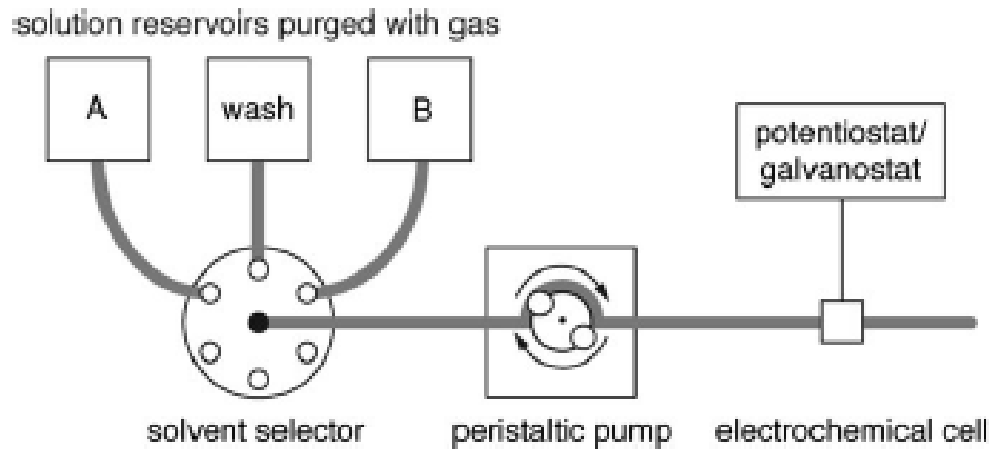
Application of Diffraction Data



Medical + Chemistry

Figure 2 WAXD patterns of the neat LDH NO₃, neat LDH Ibu, neat PLLA, and PLLA/LDH Ibu nanocomposites with different LDH Ibu loadings.

Application Example



Materials Research
Changing Properties

Fig. 1. Schematic of the flow injection instrument for multilayer deposition.

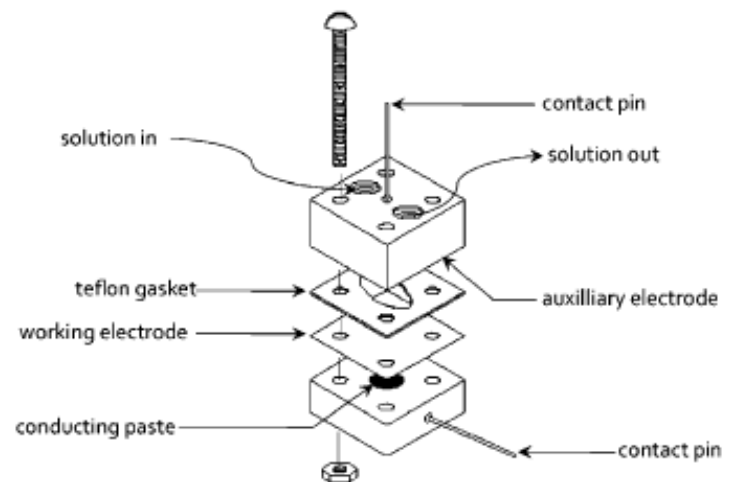


Fig. 2. Schematic of the modified flow cell electrode assembly.

Application Example

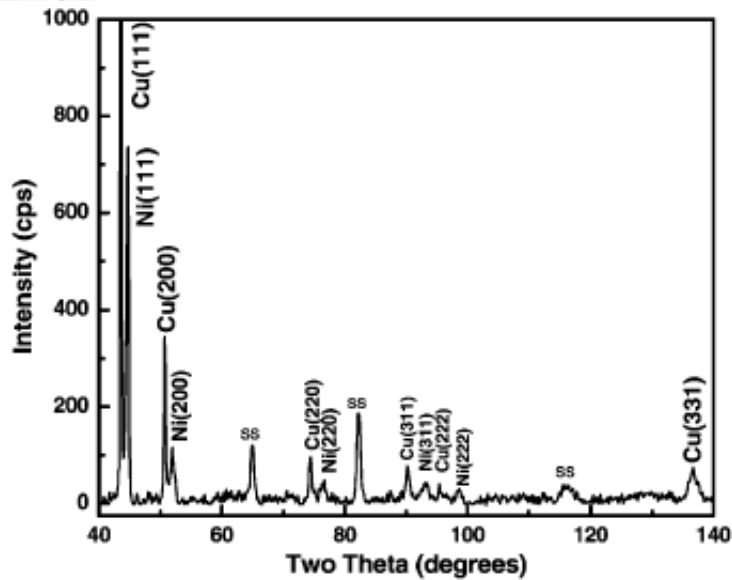


Fig. 6. XRD pattern of Ni/Cu multilayer electrodeposited at 0.25 mA/cm^2 with a total film thickness of $3.4 \mu\text{m}$ and each individual layer thickness of $0.1 \mu\text{m}$.

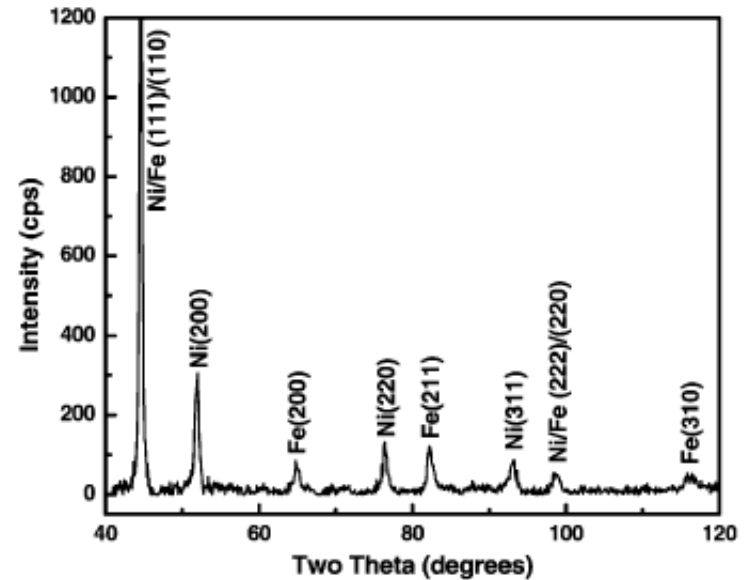
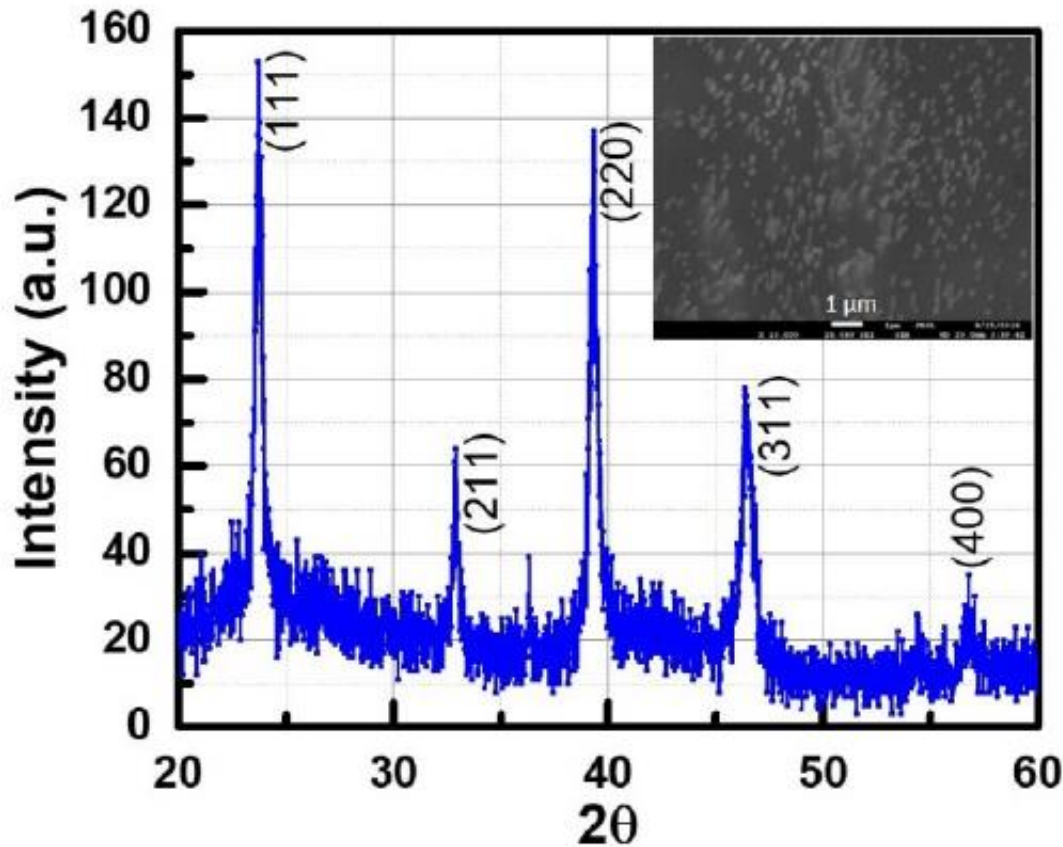


Fig. 7. XRD pattern of Ni/Fe multilayer electrodeposited at 3 mA/cm^2 with $0.5 \mu\text{m}$ layer thickness and total film thickness of $5.5 \mu\text{m}$.

Application of Diffraction Data



The inset of Figure - the SEM image from where XRD data were collected.

The InSb diffraction pattern matched the JCPDS file (00-006-0208) for a cubic zinc blende crystal structure.

The reflections ((111), (220), (311), (400)) corresponded to a random crystal structure with no preferred orientation. The lattice constant along different lattice planes was calculated and the average value was estimated to be 0.658 nm, with an average mismatch of about 1.55%.

Materials Research
Nanowires

Figure 6. X-ray diffraction (XRD) spectrum of as grown InSb nanowire in polycarbonate template.

Application of Diffraction Data

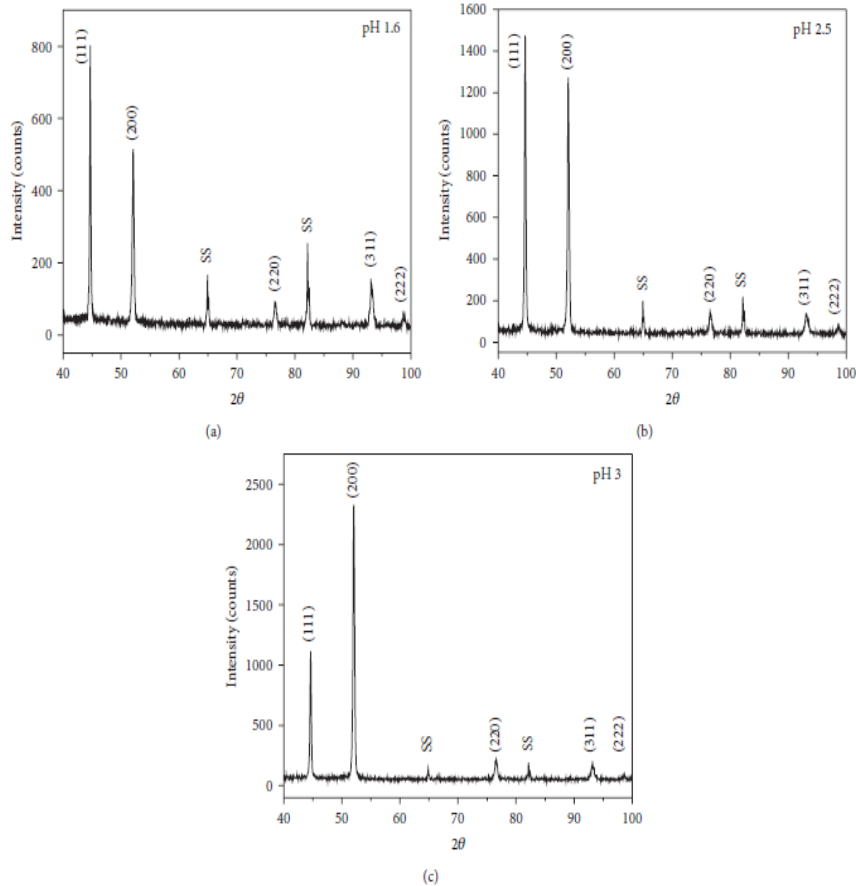


FIGURE 4: X-ray diffraction (XRD) patterns of Ni-MMT (0.5%) films electrodeposited at various pHs (a) 1.6, (b) 2.5 and (c) 3.0 (SS: substrate stainless steel peaks).

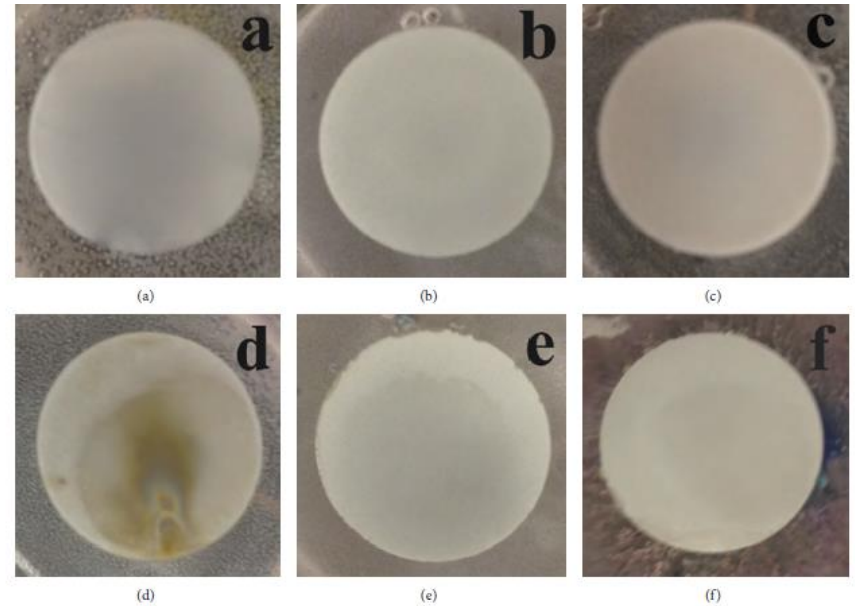


FIGURE 7: Sample images of Ni-MMT coatings electrodeposited from plating baths at various pHs of 1.6, 2.5, and 3.0 before immersion in 3.5% NaCl (a)-(c), and after (d)-(f), respectively.

Corrosion Research
Nickel-Clay

Application of Diffraction Data

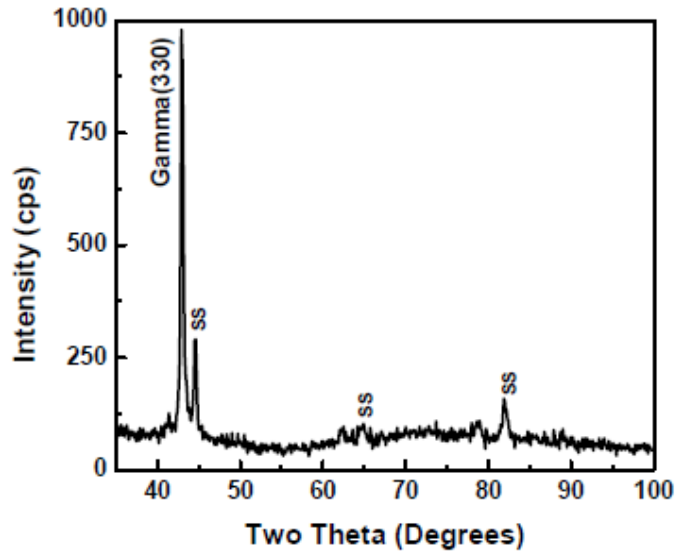


Figure 6. XRD pattern of Zn-Ni alloy film deposited from a 2:1 ZnSO₄ · H₂O: Ni(NH₄)₂(SO₄)₂ · 6H₂O solution at pH 9.36 adjusted with 1M NH₄OH.

Corrosion Research Ni-Zn

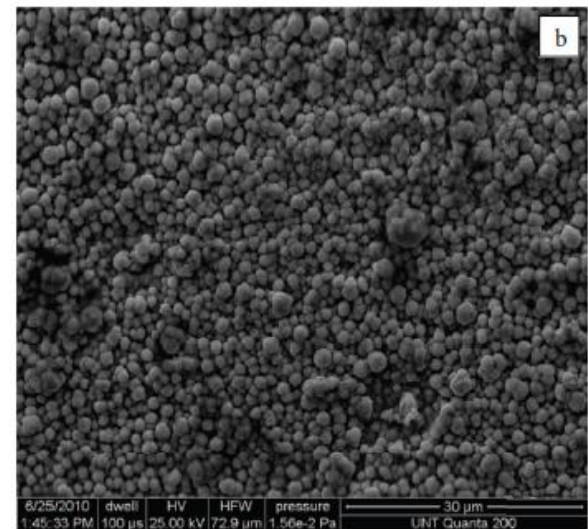
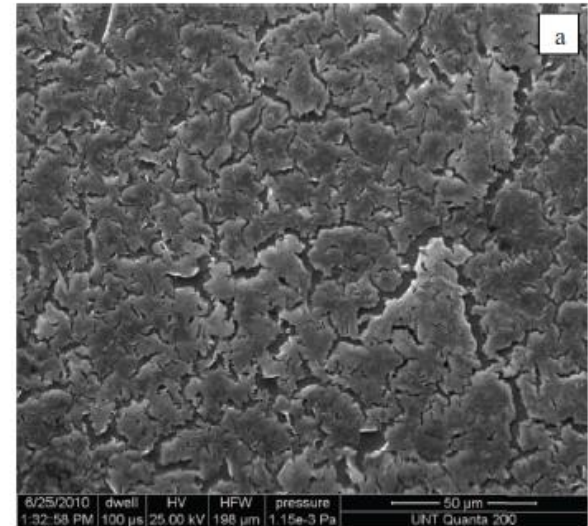


Figure 4. Scanning electron micrograph of (a) Zn-Ni film deposited from a 2:1 molar ratio bath at T = 25°C and deposited using a potential step profile of E₁ = -1.3 V for 60 s to E₂ = -1.0 V at 20 s and (b) Zn-Ni film deposited from a 2:1 molar ratio bath at T = 25°C and deposited using a potential step profile E₁ = -1.5 V for 60 s to E₂ = -1.3 V for 20 s.

Application of Diffraction Data

Corrosion Research Ni-Zn Borate

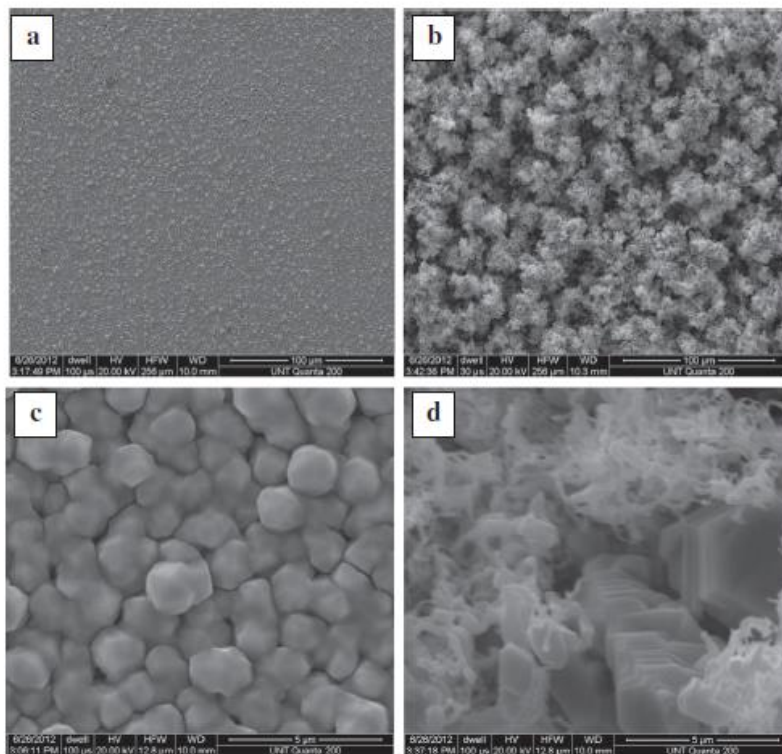


Fig 4. (a) – 2:1 ZnSO₄H₂O: Ni(NH₄)₂(SO₄)₂6H₂O ratio deposit, SEM, 100 μm, pulse potential deposition method and (b) – 2:1 ZnSO₄H₂O: Ni(NH₄)₂(SO₄)₂6H₂O ratio deposit, SEM, 100 μm, direct potential deposition method. (c) – 2:1 ZnSO₄H₂O: Ni(NH₄)₂(SO₄)₂6H₂O ratio deposit, SEM, 5 μm, pulse potential deposition method and (d) – 2:1 ZnSO₄H₂O: Ni(NH₄)₂(SO₄)₂6H₂O ratio deposit, SEM, 5 μm, direct potential deposition method.

Table 1

Corrosion data from Tafel experiments of electrochemically deposited zinc-nickel γ -phase alloy protective coatings.

| Deposit | E_{corr} (V) | i_{corr} (A) | R_p (Ω) |
|---|-----------------------|-----------------------|--------------------|
| Zn Only | -1.170 | 2.09×10^{-4} | 1333 |
| Ni Only | -0.452 | 2.75×10^{-5} | 6790 |
| Zn/Ni γ Phase (Pulse Potential) | -0.735 | 1.06×10^{-5} | 30485 |
| Zn/Ni γ Phase (Direct Potential) | -0.995 | 4.49×10^{-5} | 27942 |

Application of Diffraction Data

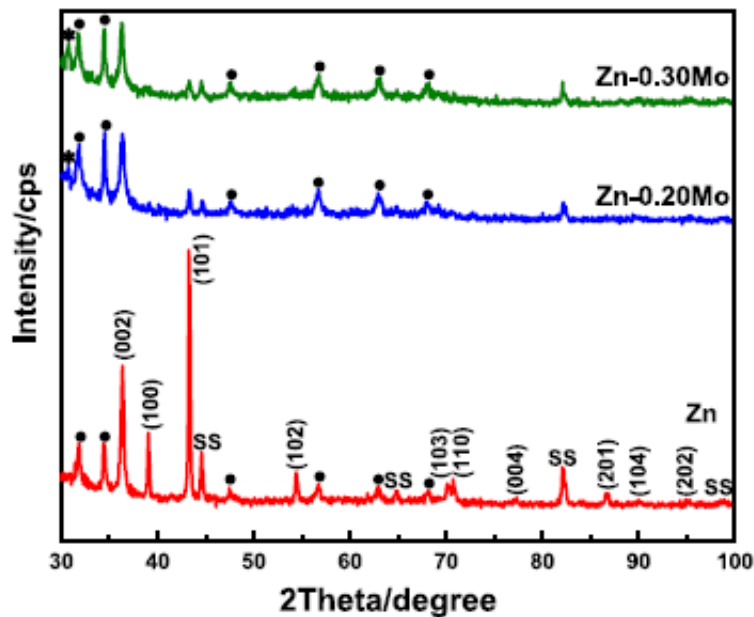


Fig. 2. X-ray diffraction patterns of as-deposited Zn and Zn-Mo coatings obtained at pH 10.0. (ZnO characteristic peaks are marked as (●), and $\text{Mo}_{17}\text{O}_{47}$ peaks are marked as (*).)

Table 2

Average crystallite size and elemental composition of as-deposited Zn-Mo coatings based on XRD and AAS data, respectively.

| Mo addition (mol/L) | Average crystallite size (nm) (n = 3) (002) reflection | Mo/Zn (at.%) in coating (n = 3) | Mo/Zn (wt%) in coating (n = 3) |
|---------------------|--|---------------------------------|--------------------------------|
| 0 | 52 (± 1.1) | – | – |
| 0.15 | 30 (± 1.6) | 3.83 (± 0.08) | 5.33 (± 0.10) |
| 0.20 | 28 (± 1.8) | 5.72 (± 0.22) | 7.75 (± 0.27) |
| 0.30 | 28 (± 3.3) | 13.76 (± 1.34) | 16.79 (± 1.36) |

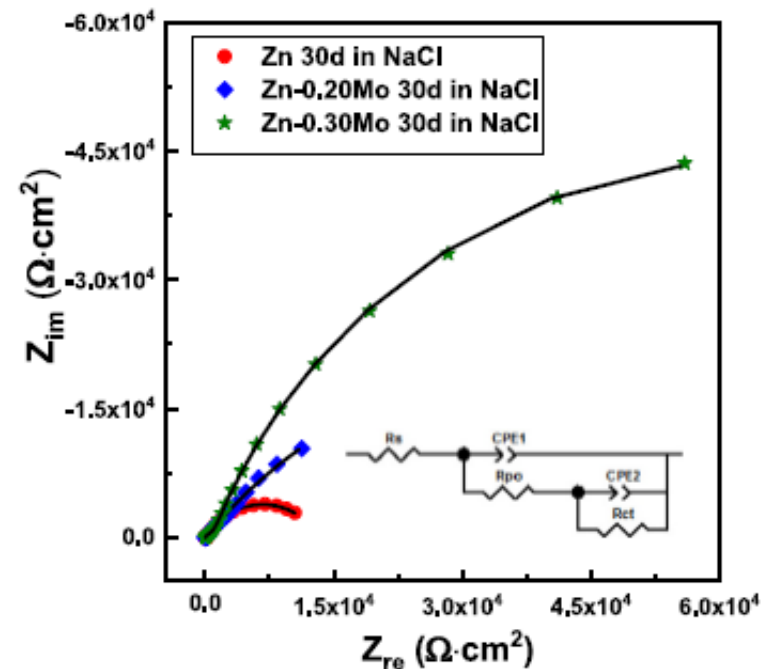


Fig. 6. Nyquist plots of Zn and Zn-Mo coatings after 30 days of submersion in 3.5 % NaCl solution.

Corrosion Research
Ni-Mo

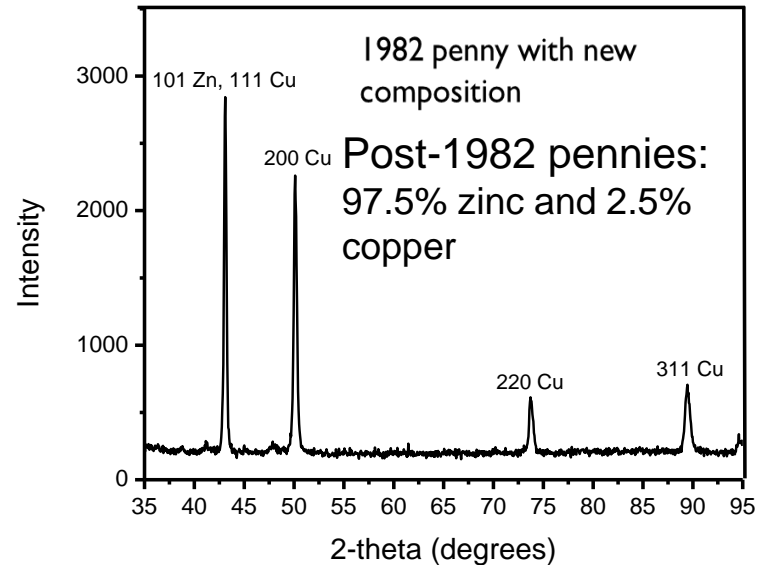
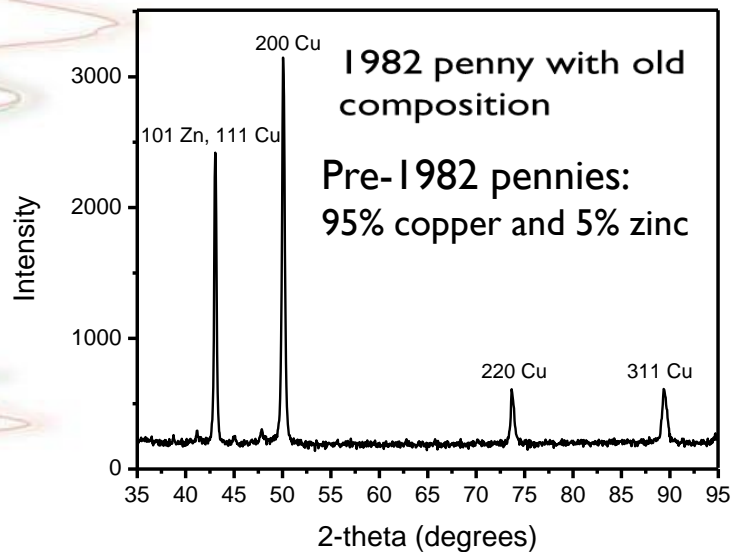
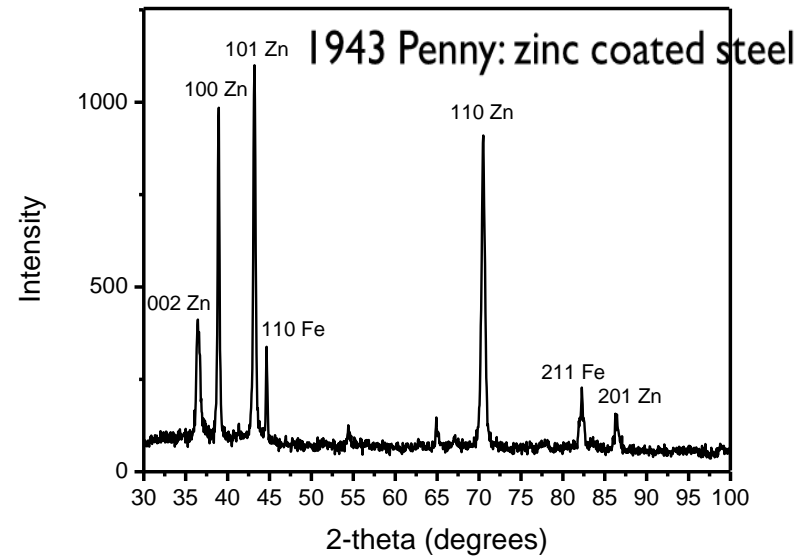
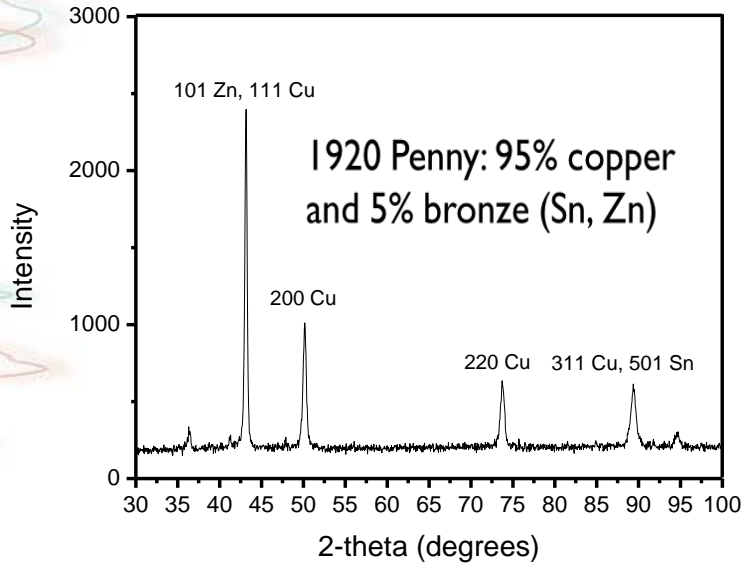
Application of Diffraction Data

Industry
Precious metals
and coinage

Composition of US Pennies

| Year | Composition |
|----------------|--|
| 1793 - 1837 | 100% copper |
| 1837 - 1857 | bronze = 95% copper, 5% tin and zinc |
| 1857 - 1864 | 88% copper, 12% nickel |
| 1864 - 1962 | bronze = 95% copper, 5% tin and zinc |
| 1943 | zinc coated steel |
| 1962 - 1982 | 95% copper, 5% zinc |
| 1982 - present | 97.5 % zinc, 2.5% copper, Cu coated Zn |

Application of Diffraction Data



Application of Diffraction Data

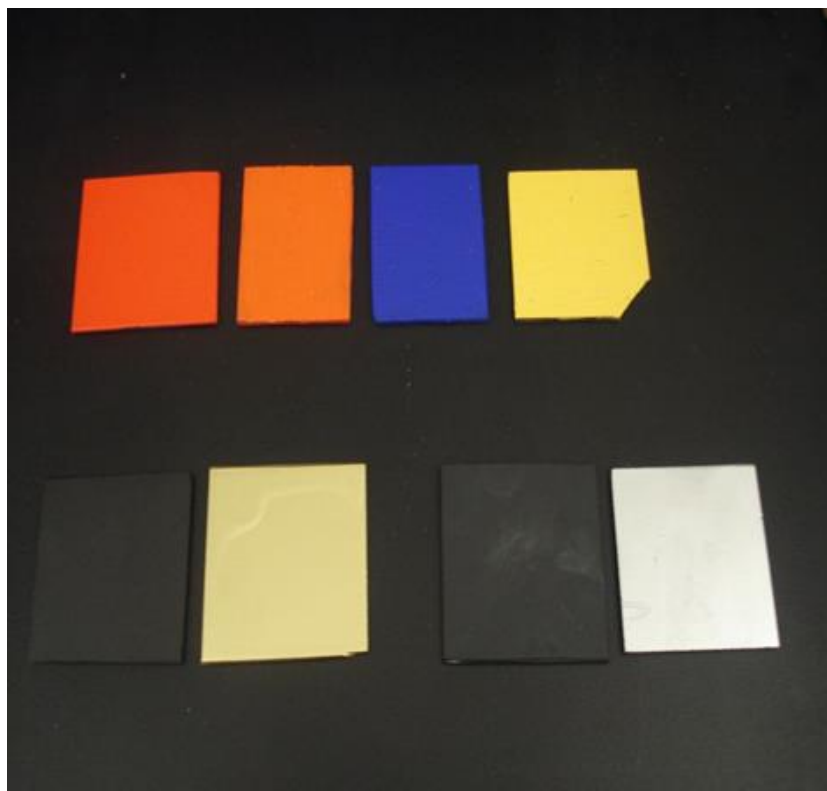
| Year | 2-theta | Intensity (I/I_0) | (hkl) |
|-------------------|---------|-----------------------|--------------------|
| Pre-1982 average | 43.2 | 98 | (111) Zn, (101) Cu |
| | 50.4 | 100 | (200) Cu |
| | 74.1 | 24 | (220) Cu |
| | 89.9 | 25 | (311) Cu |
| Post-1982 average | 43.2 | 100 | (111) Zn, (101) Cu |
| | 50.4 | 23 | (200) Cu |

Application of Diffraction Data

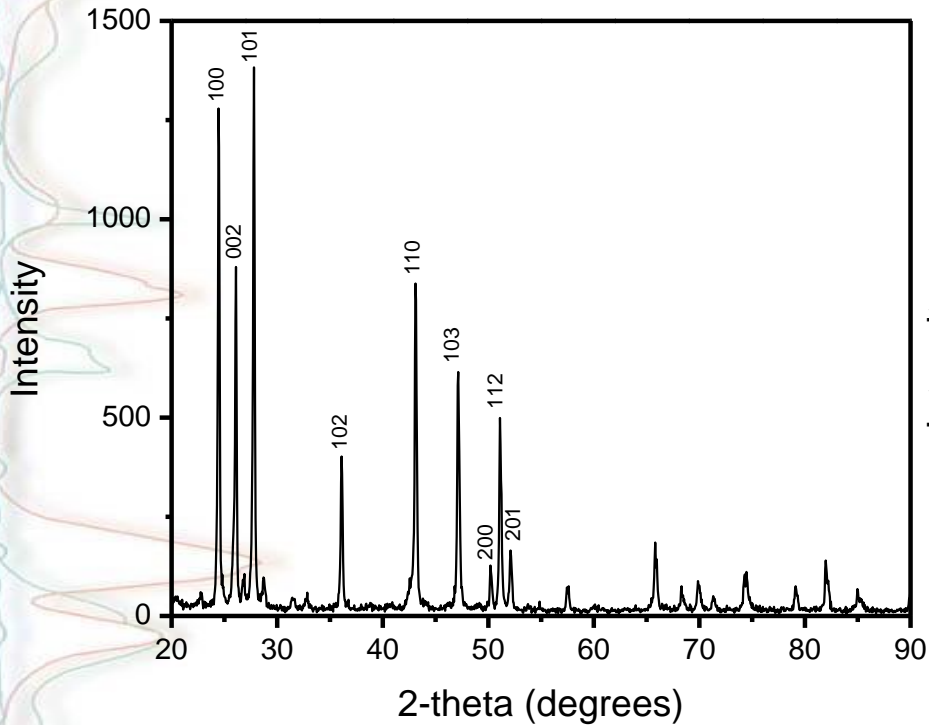
Paint Sample XRD Parameters

| Sample Color Type | Scan Range (degrees) |
|----------------------------------|---------------------------------|
| Cadmium Red Acrylic | 20-90 |
| Scarlet Red Acrylic | 20-60 |
| Cobalt Blue Acrylic | 20-100 |
| Naples Yellow Acrylic | 20-75 |
| Black Matte Spray Paint | 5-35 |
| Metallic Gold Spray Paint | 25-80 |
| Black Matte Auto Paint | 5-35 |
| Metallic Silver Auto Paint | 35-50 |

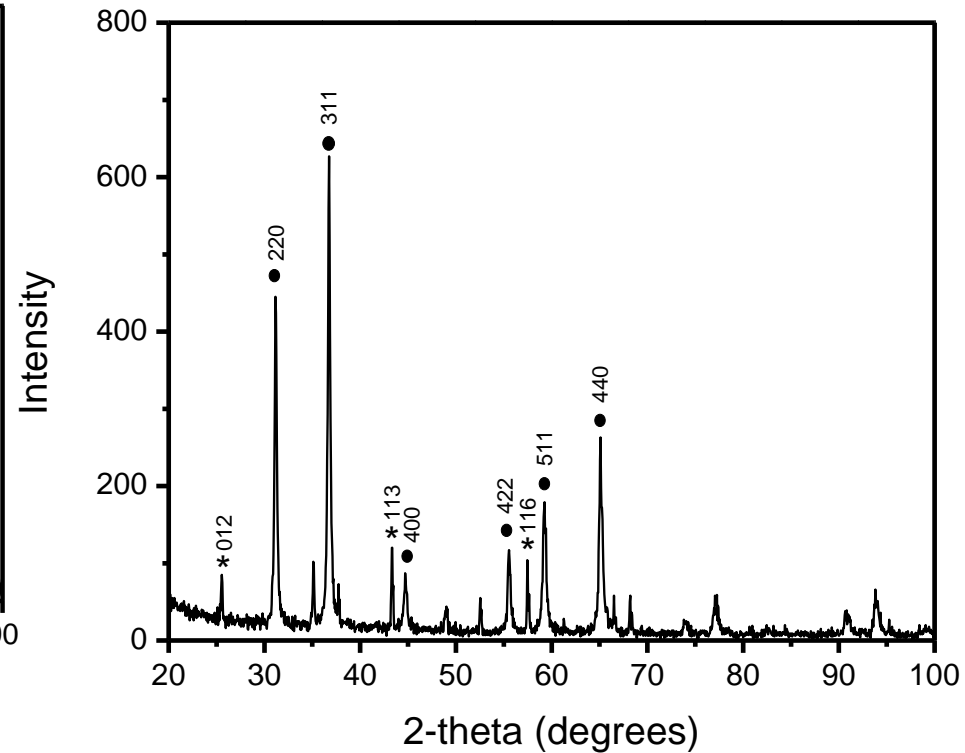
Industry
Paints, Epoxies, Polymers



Application of Diffraction Data



cadmium red acrylic paint:
cadmium selenide sulfide



cobalt blue acrylic paint: $*Al_2O_3 \cdot Co_3O_4$



Reading Assignment:

Read Chapter 3-7, 9-11 and 13 from:

-Introduction to X-ray powder

Diffractometry by Jenkins and Synder

Read Chapter 3, 4, 6, 13, and 14 from

-Elements of X-ray Diffraction

by Cullity and Stock

Read Chapter 2 from Norton

